AFRL-DE-PS-
TR-1998-1057

Design and Test of a Half Reflector Impulse Radiating Antenna with Feed-Point Lens

W. Scott Bigelow and Everett G. Farr

Farr Research, Inc.
614 Paseo Del Mar NE
Albuquerque, NM 87123

June 1998

Final Report

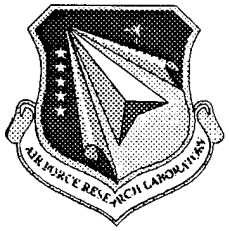

AIR FORCE RESEARCH LABORATORY
Directed Energy Directorate
3550 Aberdeen Ave SE
AIR FORCE MATERIEL COMMAND
KIRTLAND AIR FORCE BASE, NM 87117-5776

Using Government drawings, specifications, or other data included in this document for any purpose other than Government procurement does not in any way obligate the U.S. Government. The fact that the Government formulated or supplied the drawings, specifications, or other data, does not license the holder or any other person or corporation; or convey any rights or permission to manufacture, use, or sell any patented invention that may relate to them.

This report has been reviewed by the Public Affairs Office and is releasable to the National Technical Information Service (NTIS). At NTIS, it will be available to the general public, including foreign nationals.

If you change your address, wish to be removed from this mailing list, or your organization no longer employs the addressee, please notify AFRL/DEHP, 3550 Aberdeen Ave SE, Kirtland AFB, NM 87117-5776.

Do not return copies of this report unless contractual obligations or notice on a specific document requires it's return.

This report has been approved for publication.

WILLIAM D. PRATHER, DR-3
Project Manager

FOR THE COMMANDER

DR PATRICK J. VAIL, DR-4
Chief, High Power Microwave Division

R. EARL GOOD, SES
Director, Directed Energy Directorate

REPORT DOCUMENTATION PAGE

Form Approved
OMB No. 0704-0188

1. AGENCY USE ONLY *(Leave blank)*	2. REPORT DATE	3. REPORT TYPE AND DATES COVERED
	June 1998	Final Report: Jan 1996 - June 1998

4. TITLE AND SUBTITLE
Design and Test of a Half Reflector Impulse Radiating Antenna with Feed-Point Lens

5. FUNDING NUMBERS
C: F29601-96-C-0011
PE:65502F
PR:3005

TA:CO
WU:MW

6. AUTHOR(S)
W Scott Bigelow and Everett G Farr

7. PERFORMING ORGANIZATION NAME(S) AND ADDRESS(ES)
Farr Research, Inc
614 Paseo Del Mar NE
Albuquerque, NM 87123

8. PERFORMING ORGANIZATION REPORT NUMBER

9. SPONSORING/MONITORING AGENCY NAME(S) AND ADDRESS(ES)
AFRL/Phillips Site/DEHP
William D Prather / (505) 846-0416
3550 Aberdeen Avenue SE
Kirtland AFB, NM 87117-5776

10. SPONSORING/MONITORING AGENCY REPORT NUMBER
AFRL-DE-PS-TR-1998-1057

11. SUPPLEMENTARY NOTES

12a. DISTRIBUTION/AVAILABILITY STATEMENT
Approved for Public Release; Distribution is Unlimited

12b. DISTRIBUTION CODE

13. ABSTRACT *(Maximum 200 Words)*

A feed-point lens is used to match an electrically large, oil filled, coaxial waveguide to the feed arms of a high-voltage half reflector impulse radiating antenna (HIRA). Theory and designs are for rotationally symmetric lens and transmission line systems feeding reflectors having focal-length-to-diameter ratios (F/D) of 1/4. Also developed are theory and designs for systems feeding reflectors having larger F/D ratios by retaining a rotationally symmetric lens design while moving the inner feed conductor off axis. A scale-model HIRA was built to confirm the theory and design. Complex permittivity measurements were performed on the lens material. Finally, a full-size HIRA with a 24 cm diameter titanium dioxide/epoxy lens feeding a 1.83 m diameter reflector with F/D of 1/4 was built. The step response was an impulse with full width half maximum of 70 ps. The measured aperture height of the antenna was 0.36 m.

14. SUBJECT TERMS
Impulse radiating antenna; Dielectric feed-point lens; Ultra-wideband

15. NUMBER OF PAGES
44

16. PRICE CODE

17. SECURITY CLASSIFICATION OF REPORT	18. SECURITY CLASSIFICATION OF THIS PAGE	19. SECURITY CLASSIFICATION OF ABSTRACT	20. LIMITATION OF ABSTRACT
UNCLASSIFIED	UNCLASSIFIED	UNCLASSIFIED	UNLIMITED

NSN 7540-01-280-5500

Standard Form 298 (Rev. 2-89)
Prescribed by ANSI Std. 239-18
28-102

Table of Contents

List of Figures

1. Introduction

The availability of fast, single-ended, high-voltage pulsers has fueled a demand for suitable antennas to radiate the signal. A candidate antenna for this application, the Half Reflector Impulse Radiating Antenna (HIRA), was first proposed in [1], and a variation was described in [2]. The HIRA converts a plane wave in a coaxial waveguide to a spherical wave which is launched onto the conical feed arms of a (half) parabolic reflector. Upon reflection, the spherical wave is radiated as a plane wave. Normally, one would want to keep the feed point region small in order to minimize pulse distortion; but high voltages preclude that possibility. To preserve the pulse characteristics, while keeping the feed point dimensions large enough to hold off high voltages, the HIRA employs a dielectric feed-point lens to manage the conversion of the plane wave to spherical wave.

An idealized version of a HIRA feed-point lens, employing an inhomogeneous dielectric and an array of guiding conducting sheets, was described in [3]. The Phase I SBIR effort led to development of a more practical lens design, employing homogeneous dielectric material. That lens, described in [4], has a prolate spheroidal surface at the interface with the coaxial waveguide and a quartic surface of revolution at the output interface. In [5], as a part of this Phase II SBIR effort, that design was refined by linking the solution of the lens equations to the input impedance at the feed arms. Also, a figure-of-merit for the lens was defined based on maximizing the aperture integral of the electric field for the fast impulse. The analyses showed that a lens with a relative dielectric constant of 7.0 is optimal for a transition from an oil-filled coaxial waveguide to a feed point in air.

The design approach of [5] assumed a rotationally symmetric lens and conical reflector feed arm. Lens and feed shared a common axis of rotational symmetry, which was normal to the ground plane and to the axis of the reflector. This symmetry was computationally convenient, but its application was restricted to reflectors having a focal-length-to-diameter ratio (F/D) of 1/4, with the focus in the aperture plane of the reflector. This limitation was overcome in [6] by the introduction of offset feed-point designs that accommodate larger F/D ratios, while retaining the rotational symmetry of the feed-point lens. The approach described there can be thought of as a generalization of the symmetric design, in which the axis of the inner conductor of the feed is offset from the outer conductor axis. Then, the axis of the output feed cone bends to follow the path of a ray traveling along the (offset) axis of the inner conductor and through the lens. We refer the interested reader to the cited reference for the details of the theoretical basis of the offset design approach.

Since the offset designs are significantly more complex to manufacture than the rotationally symmetric design, we decided against building a nonsymmetric antenna as part of this Phase II effort. Instead, on the basis of the predictions of [5], we designed a high-voltage HIRA with feed-point lens, 1.83 m (6 ft) reflector diameter, and a focal-length-to-diameter (F/D) ratio of 1/4. This note describes that antenna, its measured impedance (TDR), its radiated field on boresight, and its characteristic step response and effective aperture height. Since a high-voltage pulser was not available, these measurements were all performed with a low-voltage source. To guide the design of this antenna and to confirm the theoretical predictions of its performance, a scale model was first constructed and tested on a ground plane in a laboratory setting. Those measurements were documented in [7], which also documented the selection and evaluation of the lens material, an epoxy paint loaded with titanium dioxide pigment. The lens material was found to have the desired relative dielectric constant of 7.0, and its breakdown strength was found adequate for pulsed high-voltage use.

The work documented in [7] demonstrated the feasibility of the full-scale high-voltage HIRA system which is the culmination of the Phase II SBIR effort and the central theme of this report. The system consists of the interface to the pulser, the high-voltage oil-filled coaxial feed, the feed-point lens, the radiating elements or feed arms, and the (half) parabolic reflector. The pulser interface was designed to provide a smooth impedance transition from the output of the Air Force Research Laboratory's H-5 pulser to the coaxial input of the HIRA. Since no high-voltage pulser was ultimately available for use in testing the HIRA, an interface to permit a coaxial cable connection to a low-voltage pulser was built instead.

The antenna step response is an impulse with a full-width-at-half-maximum (FWHM) on boresight of 70 ps. Compromises in the feed-point design contributed to impulse broadening and to a reduction in the peak field radiated on boresight. However, the effective aperture height, which is a measure of the area under the impulse, is 0.36 m. This is approximately one-half the dipole moment of the reflector, as expected. Thus, the performance of the antenna is consistent with both theory and design.

We now describe the full-scale HIRA system design and summarize measurements characterizing its performance. The material presented in this report is an abbreviated version of [8], and the reader is referred to that document for additional detail.

2. HIRA System Design

In applying the feed-point lens design approach introduced in [5], we postulate 100 Ω HIRA driven by an oil-filled coaxial transmission line with a peak driving voltage, V_0, of 2.6 MV, and a maximum permissible electric field in the transmission line, E_{max}, of 2 MV/cm. Since the relative dielectric constant of the oil is about 2.2, the impedance of the line is about 67 Ω (100 Ω in air). Although the design calculations assume a single conical feed for the half reflector, this was replaced by a pair of equivalent 200 Ω feed cones, as indicated below.

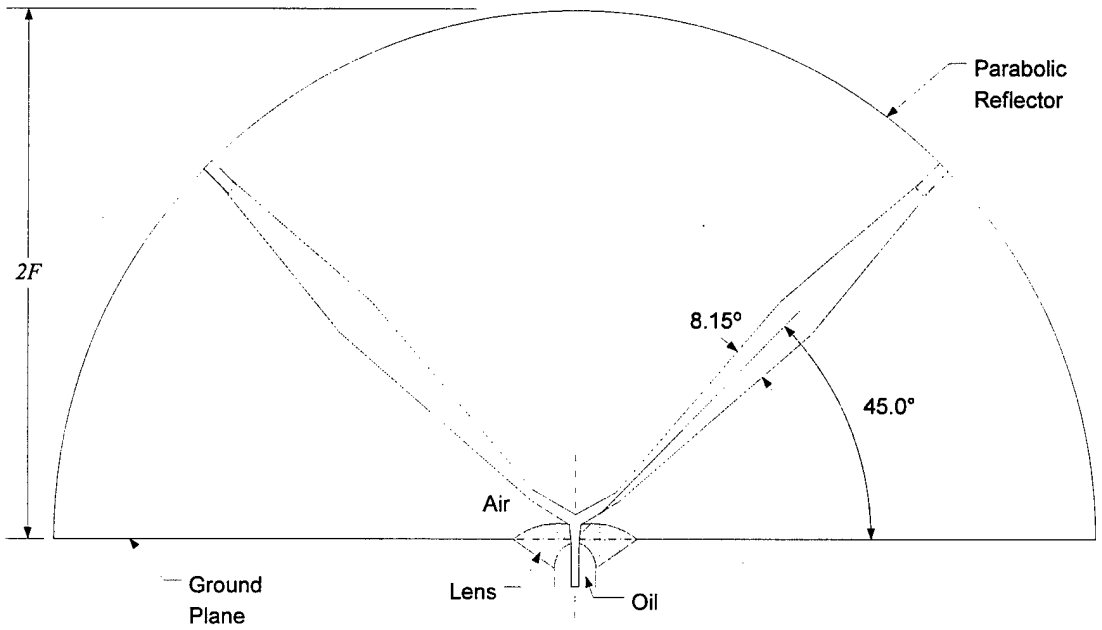

Figure 1. Concept for a two-armed HIRA with feed-point lens. In principle, the arms should intersect on the ground plane at the axis of the lens. The ratio, F/D, is 1/4.

From [9, equation (4.5)], we find that an outer coaxial conductor radius of about 4 cm will keep the electric field below our postulated maximum. From [9, equation (4.3)], the corresponding inner conductor radius is 0.75 cm. Since the relative dielectric constant of the lens material is known to be 7.0, only one additional parameter needs to be specified in order to determine the feed-point lens design. That parameter is the radius of the lens at its output on the ground plane of the half reflector. We selected a radius of 12 cm as adequate to keep the field strength sufficiently low in the space between the emerging center conductor and the ground plane, about 0.3 MV/cm.

The lens equations are solved as described in [5]. The oil-lens interface is a section of an ellipse of revolution, characterized by major semi-axis, a, and focal distance, d, with center at

$-\ell_1+\ell_2+d$. The lens-air interface is a quartic surface of revolution characterized by the distances from the intersection of that surface with the z-axis, $z=\ell_2$, to the focus of the quartic surface, $z=0$, and to the focus of the ellipsoidal surface, $z=-\ell_1+\ell_2$. In terms of these parameters, the quartic surface is formed by revolution about the z-axis of the locus of points given by [5, equation (2.1)]

$$\sqrt{\varepsilon_{r2}}\left(-\ell_1+\sqrt{\Psi^2+(\ell_1-\ell_2+z)^2}\right)=-\ell_2+\sqrt{\Psi^2+z^2} \tag{2.1}$$

where $\varepsilon_{r2}=\varepsilon_2/\varepsilon_3$, is the ratio of the relative dielectric constants of the media defining the quartic interface (lens, 7.0, and air, 1.0). The results of the calculations are summarized in the following diagram, which shows a cross section of the lens through the symmetry axis. The figure on the next page shows the top-level assembly drawings for the HIRA, along with photographs of the completed HIRA as fielded for testing. Note that the interface shown below the ground plane in the drawings is not the one which was built. The interface in the drawings was designed for connecting the HIRA to the output of the H-5 pulser.

Subsequently, Figure 5 presents photographs of the parts of the HIRA that are located below the ground plane, specifically, of the interface to the pulser, of the oil-filled coaxial input line, and of the ellipsoidal surface of the lens.

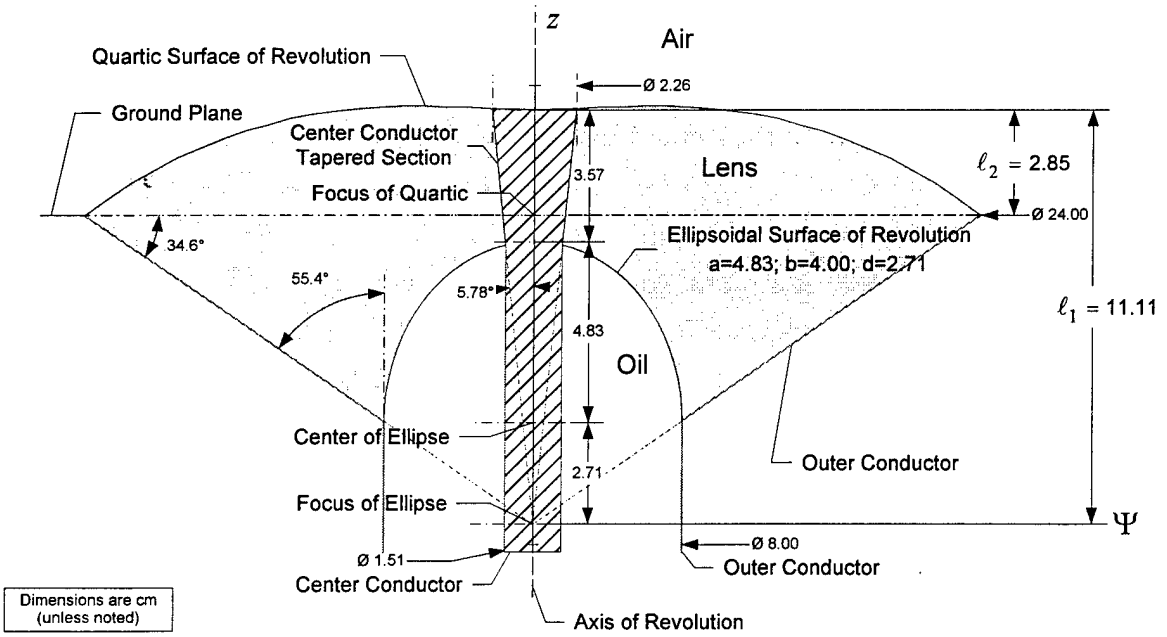

Figure 2. HIRA feed-point lens design. The relative dielectric constant of the lens is 7.0; that of the oil is 2.2; and that of air is 1.0.

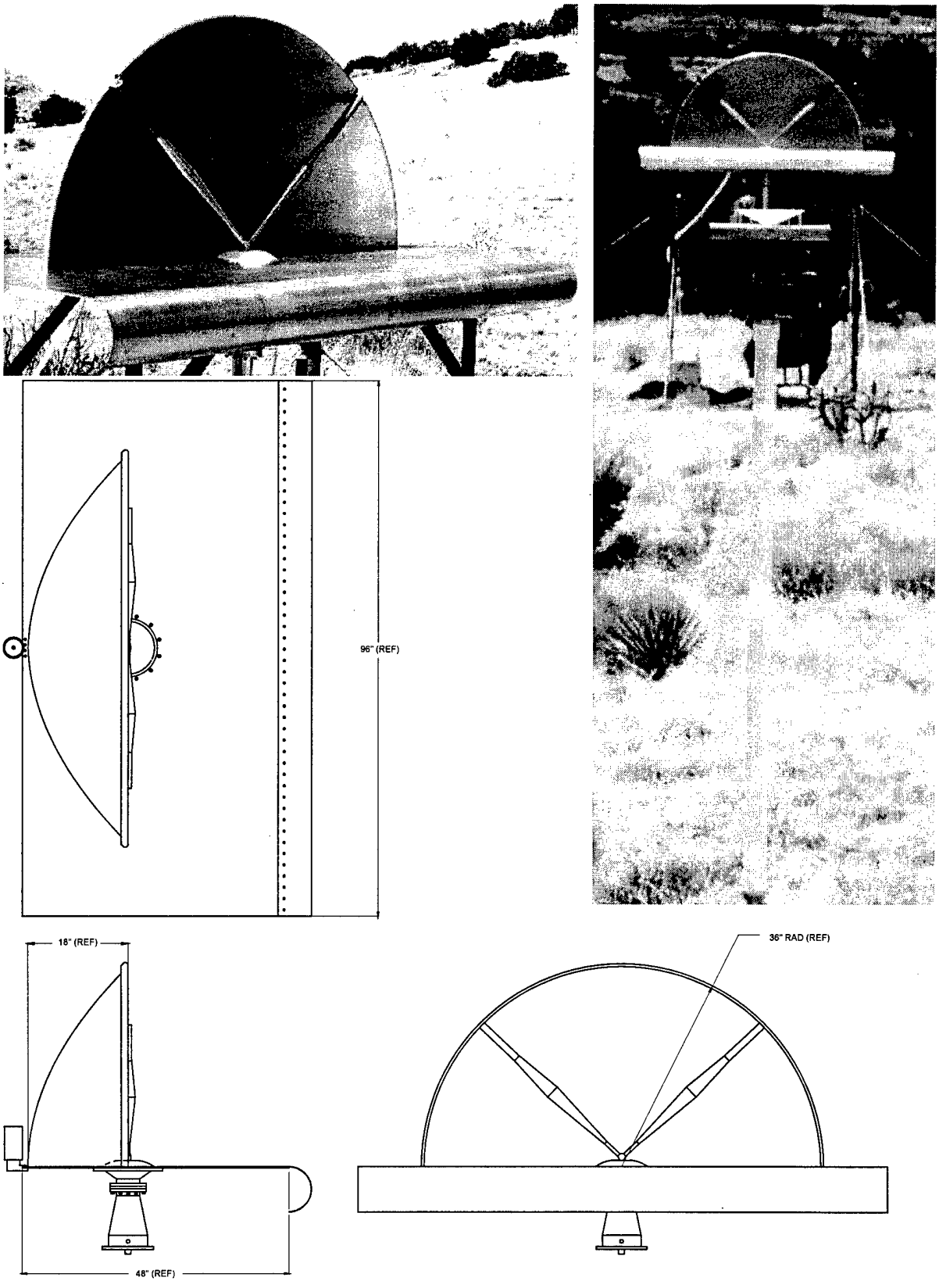

Figure 3. HIRA design and hardware.

Note also, that the feed arm design is simplified in comparison to that depicted earlier in Figure 1. In the final design, the feed arms project outward from a point above the surface of the lens, rather than from the common foci of the parabolic reflector and quartic lens surface on the ground plane at the axis of the lens. As a result, all sections of each feed arm share a common axis. This compromise in design accuracy made the feed arms considerably easier to build. Each arm was made by turning a single piece of stock on a lathe. The following figure shows the feed arm detail. The design is similar to that used in the scale-model HIRA, as reported in [7]. As

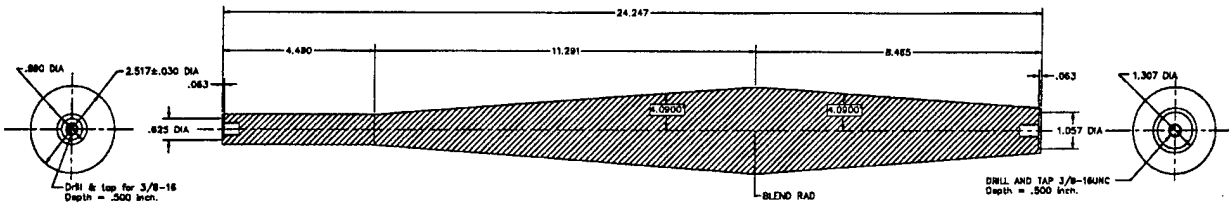

Figure 4. Feed arm section details.

explained there, the taper reversal helps to keep the impedance from sagging as the arm nears the grounded surface of the reflector. The most notable difference from the scale-model design is the cylindrical section at the lens end, where the feed arm connects to the "Y" that joins it to the other feed arm and to the end of the center conductor. This approach helps to keep the conductor radii large enough to ensure mechanical stability.

Figure 6 shows close-up photographs of both the full-scale and scale-model HIRAs. The differences and similarities in feed arm geometry are readily apparent. Note also that in both HIRAs, each feed arm is resistively terminated in a matched load. In the full-scale HIRA, each feed arm is terminated at the reflector through a 200 Ω network of Dale NS-10, wire-wound, 100 Ω resistors. Two parallel strings of four resistors in series comprise each terminator.

3. HIRA Testing

The HIRA was assembled for outdoor testing in a remote area northwest of the Air Force Research Laboratory's HERTF on Kirtland AFB. Test equipment included a modified Picosecond Pulse Labs Model 4600 step generator, which produced a nominal 21 V step at 50 Ω, a Tektronix 11801B digital sampling oscilloscope with SD24 sampling/TDR head and 2 m extender cable, and a prototype of the standard Farr Research 50 Ω replicating TEM sensor. Also available were interconnecting RF signal cables, trigger cable, and calibrated high-voltage RF attenuators. A portable generator supplied power for the test equipment. A 9X telescopic sight with an aluminum channel mount was used as an aid to antenna and sensor alignment.

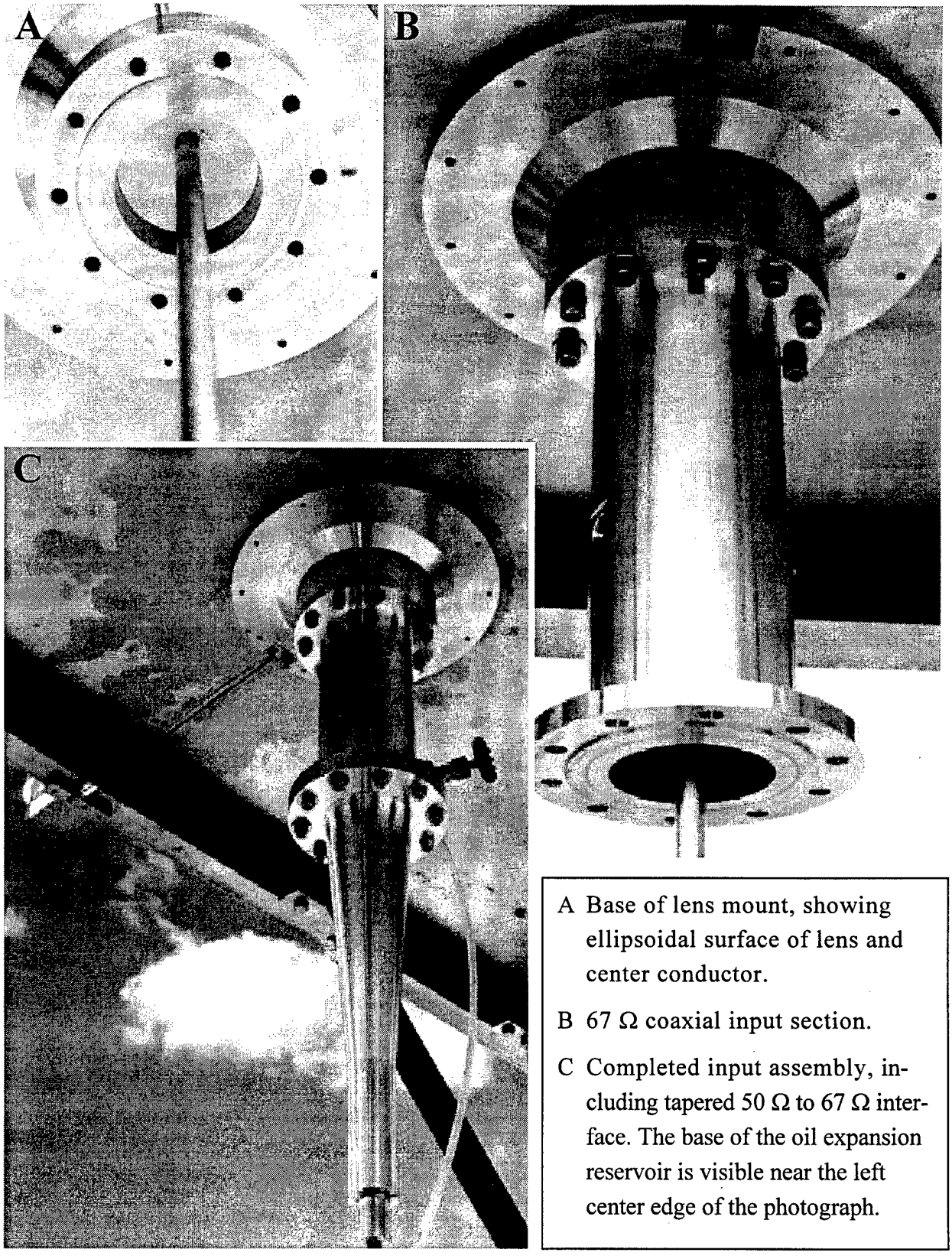

A Base of lens mount, showing ellipsoidal surface of lens and center conductor.

B 67 Ω coaxial input section.

C Completed input assembly, including tapered 50 Ω to 67 Ω interface. The base of the oil expansion reservoir is visible near the left center edge of the photograph.

Figure 5. HIRA components located below the ground plane.

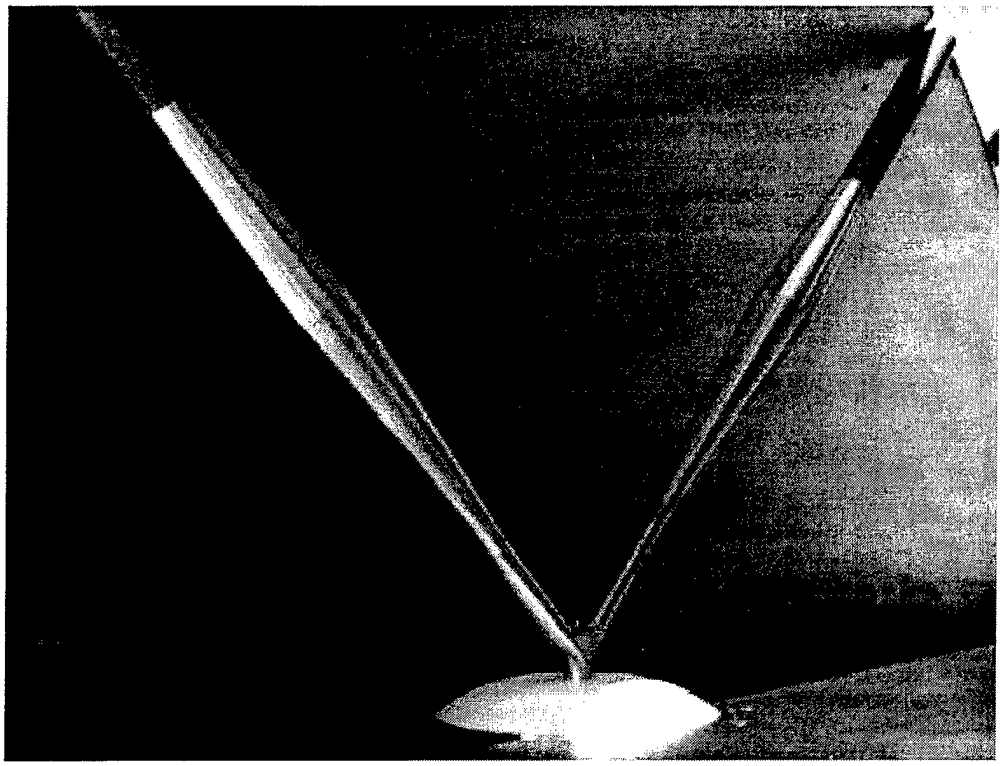

A. Full Scale HIRA

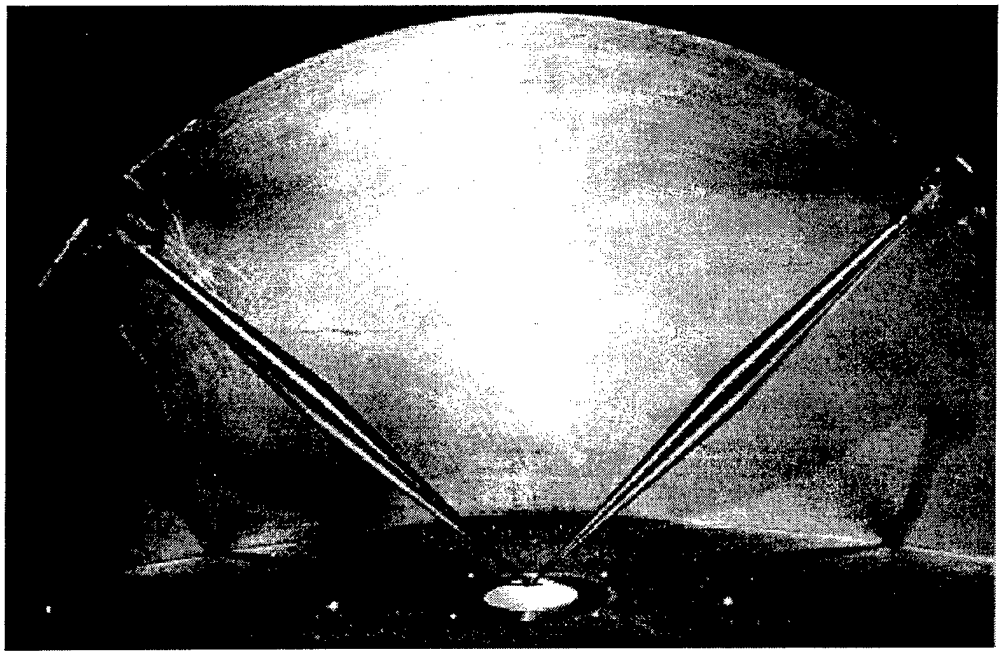

B. Scale-Model HIRA

Figure 6. Photographs of HIRA feed arm details.

3.1 Impedance Measurement

The impedance of the HIRA system was measured with the Tektronix 11801B by driving the antenna through a 2 ft semi-rigid coax with the 30 ps step pulse of the SD24 sampling head. The resulting TDR is shown below in Figure 7, along with annotations identifying the parts of the system responsible for the observed features. The lens assembly accounts for a relatively brief but large impedance discontinuity. Although this HIRA TDR profile closely parallels that of the scale-model HIRA shown in [7, Figure 5-4], there are several differences. For example, the larger size of the HIRA permits the SD24 TDR pulse to better resolve impedance fluctuations. Also, there is a shoulder on the rising portion of the profile corresponding to the exit from the lens; and the impedance rises to 115 Ω before declining. This behavior may be caused by a combination of the "Y" connector for the feed arms and the cylindrical sections at the base of each feed arm.

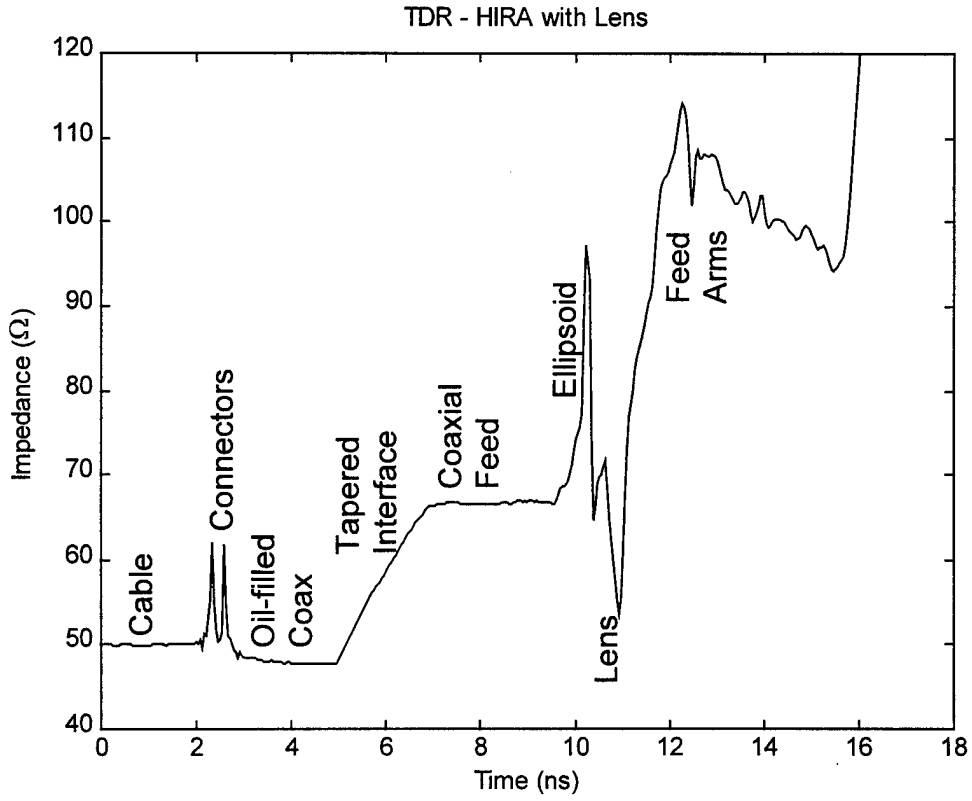

Figure 7. Impedance of the HIRA assembly.

3.2 Radiated Electric Field Measurements

3.2.1. Test Site Configuration

Figure 8 depicts the arrangement of the HIRA and TEM sensor for radiated electric field measurements. The ground at the test site was packed dry soil with typical desert vegetation (Figure 3). The surface was mostly flat, with a slight uphill grade from the HIRA to the sensor locations. The HIRA ground plane was mounted on an adjustable Unistrut® frame at a height of approximately 2.78 m. The sensor was mounted on a tripod with extended elevator section at a height of 2.43 m. The frame holding the HIRA was tipped so that the boresight would run approximately parallel to the ground surface. A 9X telescopic sight mounted on the HIRA ground plane was used in adjusting the sensor to a position directly on boresight. Then, the telescopic sight was moved to the sensor ground plane and used to align the sensor with the boresight direction.

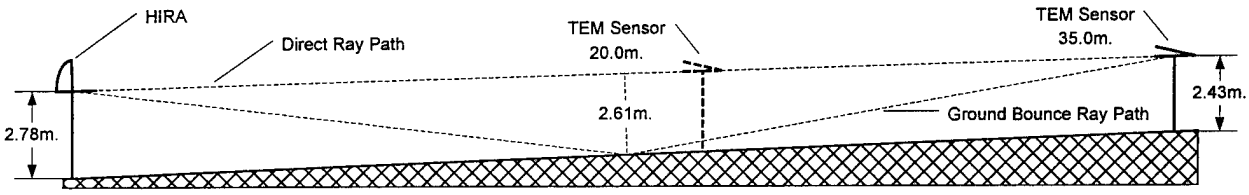

Figure 8. Physical layout of HIRA and TEM sensor for radiated field measurements. The time-of-flight for the ground bounce path is 1.3 ns longer than the direct path when the sensor is 35 m from the HIRA; it is 2.2 ns longer when the sensor is at 20 m.

3.2.2. Test Equipment Configuration

The experimental test configuration for the HIRA measurements is shown below in Figure 9. The Picosecond Pulse Labs 4600 step generator drives the HIRA through a type SMA connector mounted at the base of the oil-filled input section (Figure 5C). The length of the interconnecting cable was 1.9 m. On the receive end, the Farr Research TEM sensor receives the signal, which is then passed through the 8.6 m signal cable and sampled by the SD24 sampling head and the Tektronix 11801B digital sampling oscilloscope. The signal to trigger the 11801B was supplied by the step generator. The rather long signal cable on the receive end provided additional delay to permit the 11801B to synchronize reliably with the step generator.

The TEM sensor was calibrated previously, as described in [10].The step generator output and its derivative, as seen through the 10.5 m total signal cable length, are shown below in

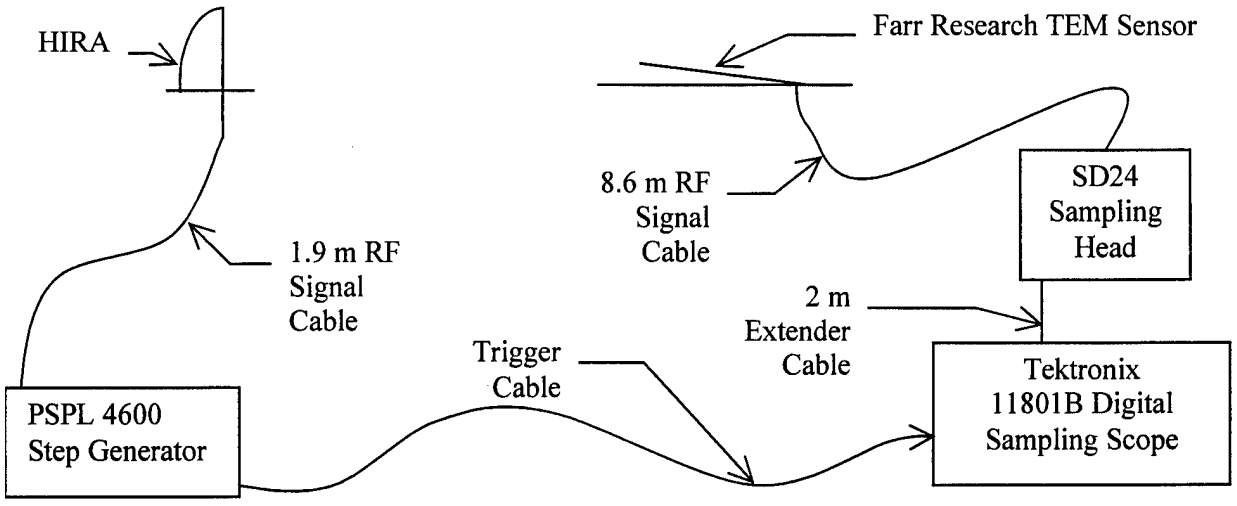

Figure 9. Experimental test setup for measuring HIRA radiation characteristics.

Figure 10. The long cables lead to a 5% attenuation of the step height to 19.5 V, and nearly double the FWHM of the derivative from 75 ps to 140 ps. The cable effects have no significant impact on determination of the HIRA step response, however, as both the source and the sensor response are deconvolved from the raw data during signal processing.

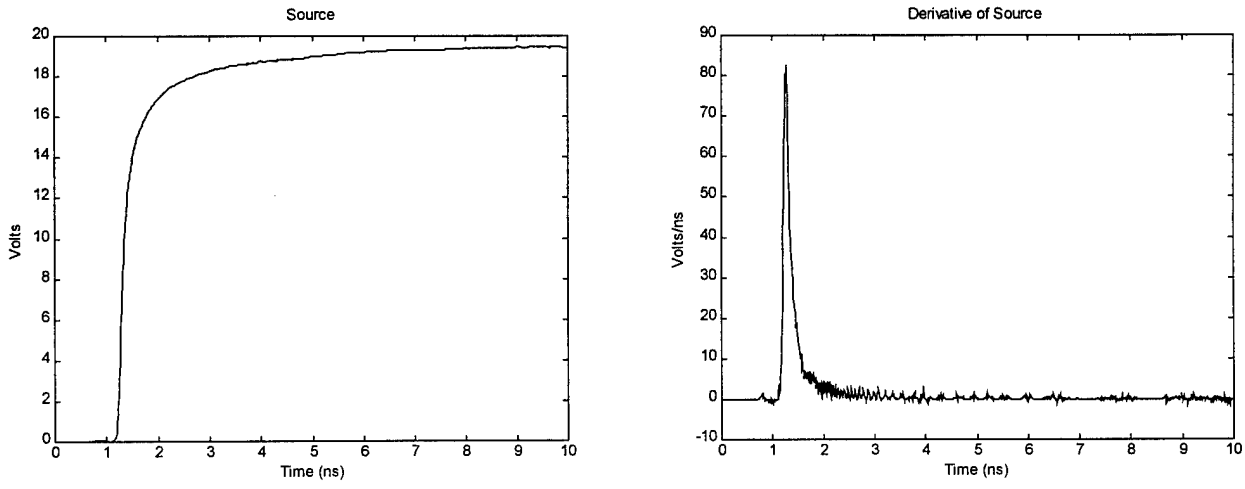

Figure 10. Voltage step and its derivative, through a 10.5 m length of RF cable. The maximum height of the step is 19.5 V. The FWHM of the derivative is about 140 ps.

3.2.3. Signal Processing

The voltage waveform as received by the SD24 sampling head contains contributions from the sensor impulse response, the HIRA step response, and the driving step function source. From [8] we know that the time-dependent received voltage at the sampling head can be represented as the convolution of the derivative of the source supply voltage with the sensor impulse response and the antenna step response, as

$$V^{rec}(r,t) = \frac{\tau_{SENSOR}\tau_{HIRA}}{(2\pi c f_g r)} \frac{dV^{src}(t)}{dt} \otimes h_{SENSOR}(t) \otimes h_{HIRA}(t) \tag{3.1}$$

where

τ_{SENSOR} is the transmission coefficient from the impedance of the sensor (50 Ω) to the 50 Ω impedance of the cable at the output of the sensor ($\tau_{SENSOR} = 1.0$),

τ_{HIRA} is the transmission coefficient from the 50 Ω feed cable impedance to the 100 Ω impedance of the HIRA feed arms ($\tau_{HIRA} = 1.33$), and

f_g is the normalized impedance of the antenna ($f_g = 0.2654$).

By deconvolving the sensor response from the received voltage, we can obtain a measure of the radiated electric field, $E^{rad}(r,t)$, at the sensor location, which, in the absence of background, is just the field incident upon the sensor, $E^{inc}(r,t)$. Furthermore, by deconvolving both the sensor response and the source derivative from the received voltage, we can obtain the HIRA step response.

Since a convolution with an impulse-like function can be approximated by a multiplication by the area under the impulse, we can define an effective aperture height for the antenna by

$$E^{rad}(r,t) \approx \frac{\tau_{HIRA}\, h_{eff}}{(2\pi c f_g r)} \frac{dV^{src}(t)}{dt}$$
$$h_{eff} = \int_{\text{Impulse}} h_{HIRA}(t)dt \tag{3.2}$$

From symmetry arguments, the integral in (3.2) is also one half of the dipole moment of the HIRA, or $a/(2\sqrt{2})$, where a is the radius of the reflector. This can be used to predict HIRA performance.

3.2.4. Test Protocol and Data Analysis

Measurements of the electric field radiated by the HIRA were made on boresight at distances of both 35 and 20 meters from the focus of the reflector, as indicated previously in Figure 8. Data were also obtained at representative offsets from boresight. Signal processing generally employed the techniques of [11, Section III], and followed the approach outlined above. Ground bounce and later contributions to the received waveforms were time-gated out prior to any other signal processing.

In presenting the radiated field obtained by deconvolving the sensor response from the received voltage, we use rE^{rad}/V_o, where V_o is a reference voltage. In the far-field,† this normalized function is independent of the range, r. In the time domain, it is dimensionless; in the frequency domain, its units are 1/GHz. For the reference voltage, we choose the maximum of the voltage step applied at the feed arms. From Figure 10, the maximum voltage at the HIRA input, $V_{\max}^{src}$, is 19.5 V. Thus, from $V_o = \tau_{HIRA}\, V_{\max}^{src}$, we obtain 25.9 V at the feed arms.

The normalized radiated field data are presented in Figure 11. The impulse maxima are approximately equal for both 35 m and 20 m ranges, as we would expect for far-field measurements. The magnitude, 2.0, is about half the predicted value for our driving source [12, equation (5.1), *et seq.*]. The primary cause of this is probably the minor offset (discussed above, on page 6, and shown in the photograph of Figure 6A) between the apparent intersection of the feed arms (above the lens) and the focus of the reflector (on the ground plane). This design compromise leads to some broadening of the radiated impulse, thus reducing its maximum.

Next, the data are processed to extract $h_{HIRA}(t)$, the HIRA response to a step input. These step response results are presented in Figure 12. On boresight, we see an impulse with a FWHM of about 70 ps and maximum in the 3.2 to 3.8 m/ns range. As with the normalized fields, the on-boresight step response should be independent of range. Finally, in Figure 13, we provide the integral of this impulse. From (3.2), the jump in the integral of $h_{HIRA}(t)$ gives us the effective

† Specification of what constitutes the far-field for an impulse field is open to some discussion. As a working definition, we assume that a range greater than $3a^2/2ct_r$, where a is the reflector radius, is in the far-field. For a gaussian impulse, the rise time is about 1.09 times the FWHM [12]. The FWHM of our source is about 140 ps, leading to a far-field range of 27 m. The FWHM of the radiated impulse is at least 212 ps, corresponding to a far-field range of only 18 m. On the basis of these observations, it appears safe to conclude that our 20 m measurement location was at the near edge of the far-field, while the 35 m measurements were clearly within the far-field.

aperture height of the HIRA, h_{eff}. On boresight, we obtain approximately 0.36 m. Since the reflector radius is 0.9144 m (36 inches), we expect to see $0.9144/(2\sqrt{2}) = 0.32$ m. Thus, our h_{eff} is about 11% higher than expected; and we conclude that our measurement is consistent with theory.

The following table summarizes the results of the HIRA measurements.

Range	Position Relative to Boresight		Radiated Field (Normalized)		Step Response		Effective Aperture
(meters)	Distance (meters)	Angle (degrees)	Peak	FWHM (ps)	Peak (m/ns)	FWHM (ps)	Height (meters)
35.	0.	0.	2.00	212.	3.76	70.	0.359
	0.6	1.	1.86	230.	2.94	84.	0.363
	1.2	2.	1.60	275	1.84	170.	0.356
20.	0.	0.	1.87	222.	3.22	76.	0.352
	1.6	5.	1.03	482.	0.88	300.	0.349

4. Conclusions

The measured effective aperture height of the antenna is approximately 11% greater than the theoretical value. The antenna step response is an impulse with a FWHM on boresight of 70 ps. As a result of impulse broadening arising from compromises in the feed-point design, the peak electric field radiated on boresight is reduced. This has no effect, however, on the area under the impulse. We conclude that the HIRA performance is consistent with both theory and design.

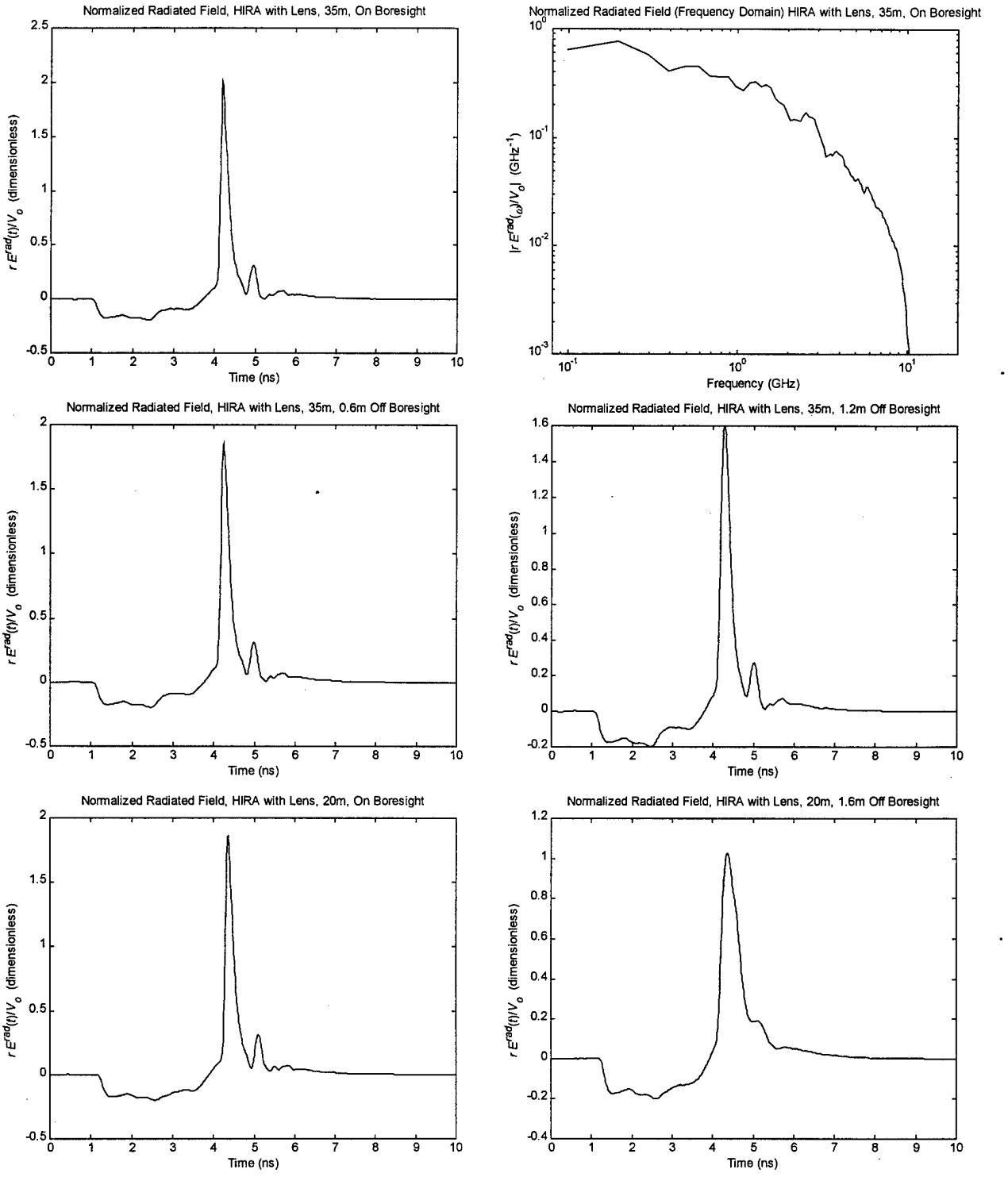

Figure 11. Normalized radiated electric fields at 35 and 20 meter ranges, both on and off boresight. The reference voltage, V_o, is 25.9 volts.

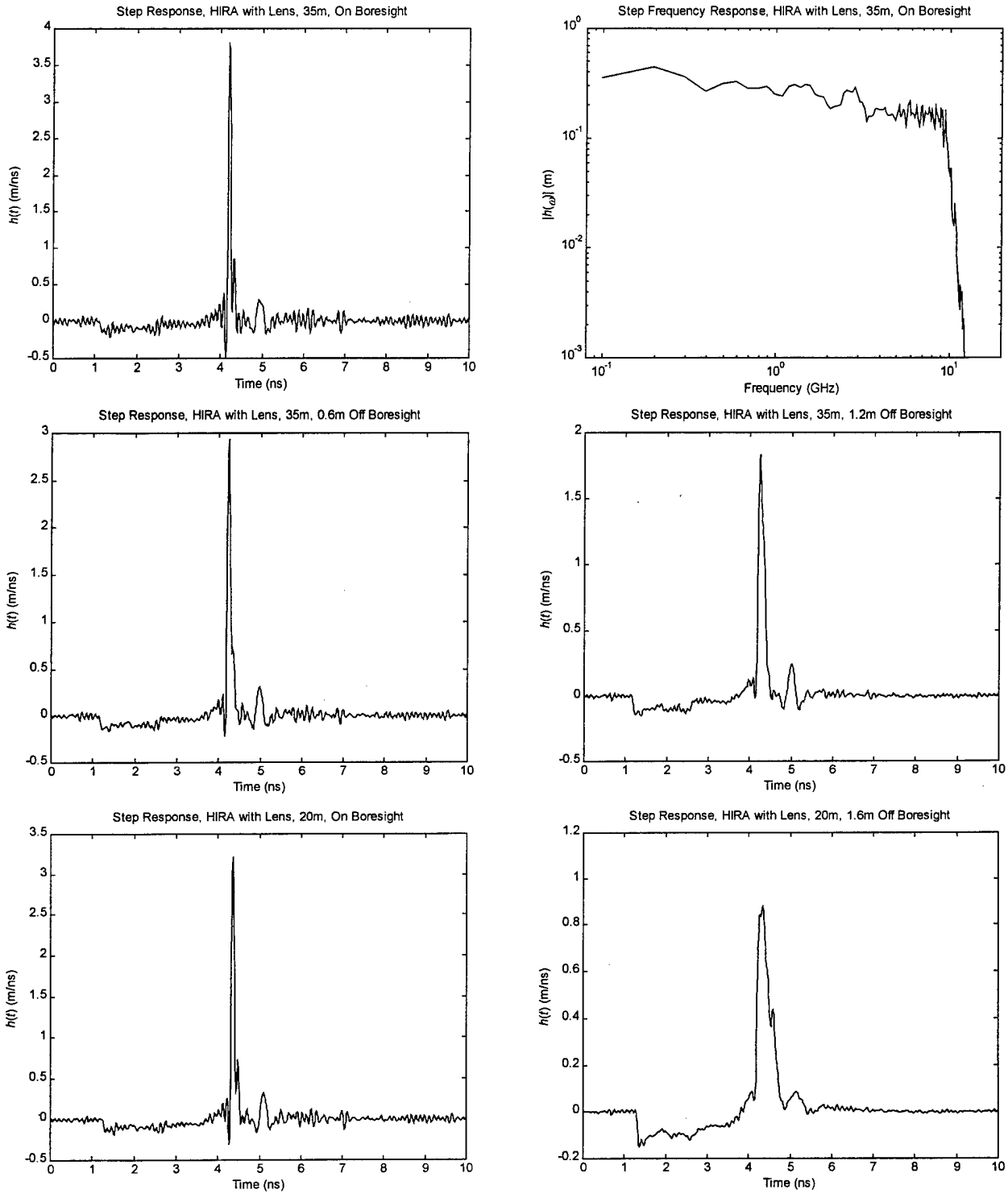

Figure 12. Step response of the HIRA, as observed from 35 and 20 meter ranges, both on and off boresight.

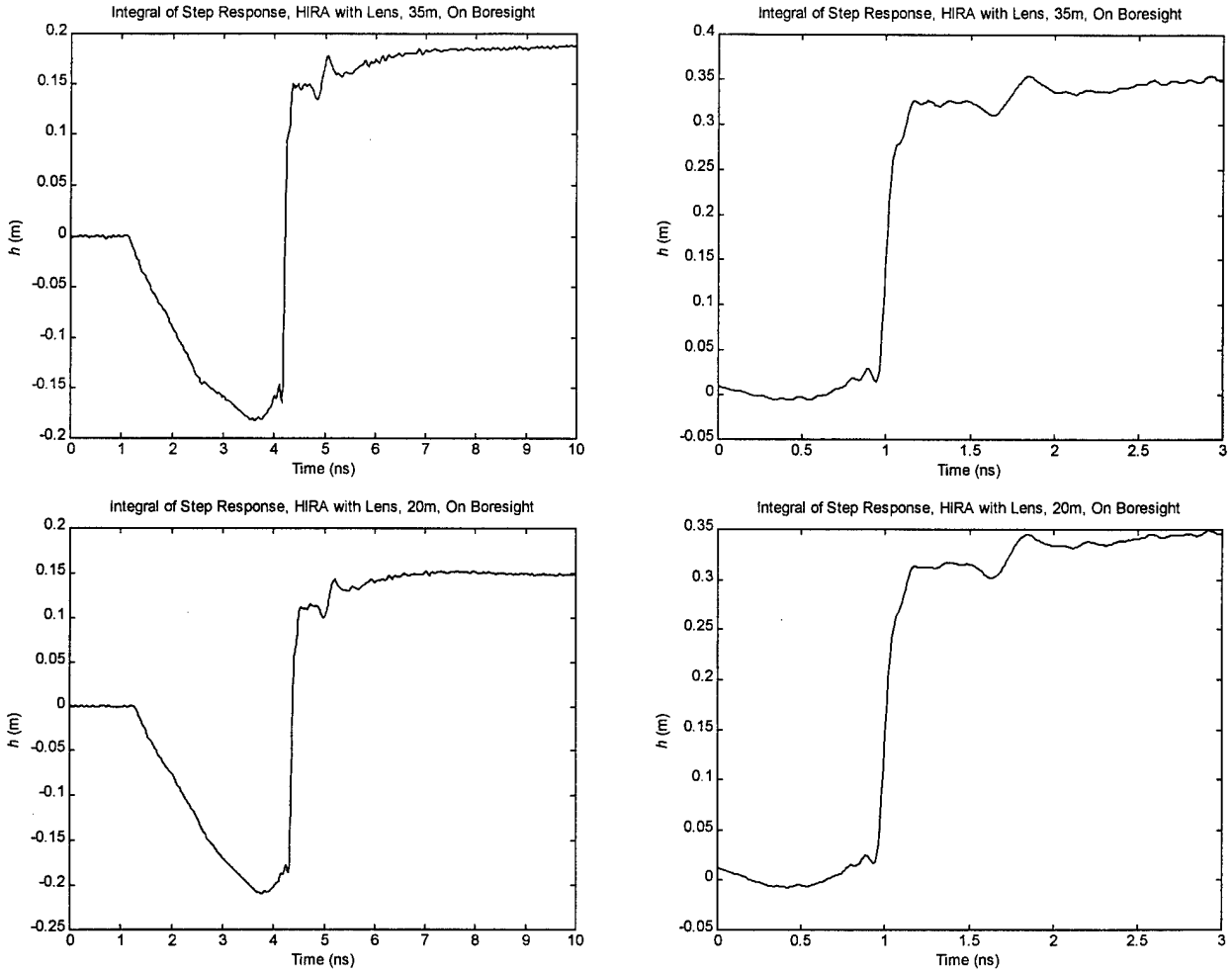

Figure 13. Integral of HIRA step response, as observed at 35 and 20 meter ranges, on boresight. The jump in the integral is the effective aperture height. It is the area under impulse of $h_{HIRA}(t)$.

References

1. C. E. Baum, *Variations on the Impulse-Radiating Antenna Theme*, Sensor and Simulation Note 378, February 1995.

2. E. G. Farr and C. E. Baum, *Impulse Radiating Antennas with Two Reflecting or Refracting Surfaces*, Sensor and Simulation Note 379, May 1995.

3. C. E. Baum and A. P. Stone, *Transient Lens Synthesis: Differential Geometry in Electromagnetic Theory*, Appendix I, Taylor and Francis, New York, 1991.

4. E. G. Farr and C. E. Baum, *Feed-Point Lenses for Half Reflector IRAs*, Sensor And Simulation Note 385, November 1995.

5. W. S. Bigelow, E. G. Farr, and G. D. Sower, *Design Optimization of Feed-Point Lenses for Half Reflector IRAs*, Sensor and Simulation Note 400, August 1996.

6. W. S. Bigelow and E. G. Farr, *Design of a Feed-Point Lens with Offset Inner Conductor for a Half Reflector IRA with F/D Greater than 0.25*, Sensor and Simulation Note 410, September 1997.

7. G. D. Sower, L. M. Atchley, D. E. Ellibee, W. S. Bigelow, and E. G. Farr, *Design for Half Impulse Radiating Antennas: Lens Material Selection and Scale-Model Testing*, Measurement Note 54, February 1998.

8. W. S. Bigelow, E. G. Farr, G. D. Sower, and D. E. Ellibee, *Design and Test of a Half Reflector IRA with Feed-Point Lens*, Sensor and Simulation Note, to be published June 1998.

9. E. G. Farr, G. D. Sower, and C. J. Buchenauer, *Design Considerations for Ultra-Wideband, High-Voltage Baluns*, Sensor and Simulation Note 371, October 1994.

10. E. G. Farr, C. E. Baum, and W. D. Prather, *Multifunction Impulse Radiating Antennas: Theory and Experiment*, Sensor and Simulation Note 413, November 1997.

11. E. G. Farr and C. A. Frost, *Compact Ultra-Short Pulse Fuzing Antenna Design and Measurements*, Sensor and Simulation Note 380, June 1995.

12. E. G. Farr and G. D. Sower, *Design Principles of Half Impulse Radiating Antennas*, Sensor and Simulation Note 390, December 1995.

NOTE: Break all edges

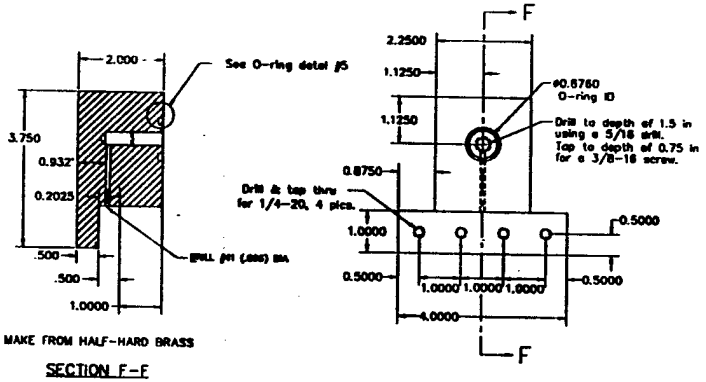

UPPER EXPANSION BLOCK ①
(part #7)

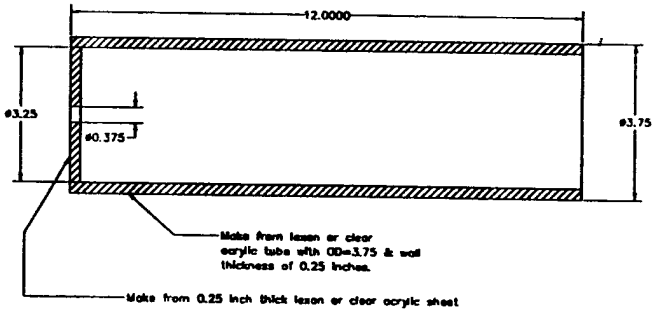

OIL EXPANSION CHAMBER ③
(part #8)

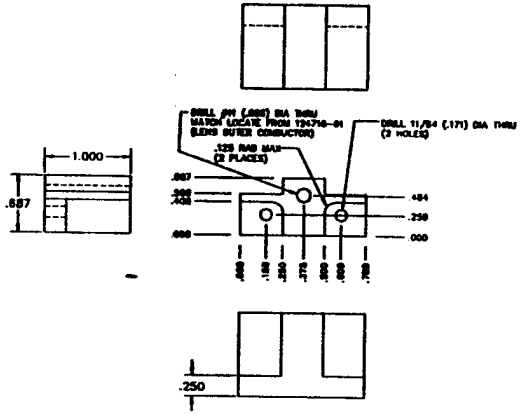

LOWER EXPANSION BLOCK ②
(part #6)

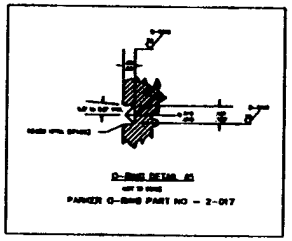

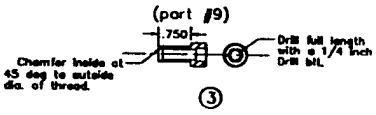

		8090	MSI
			HIRA OIL EXPANSION SYSTEM
		E 29674	124711

NOTE:
1 – Break all edges
2 – MATERIAL = ALUM ALLOY

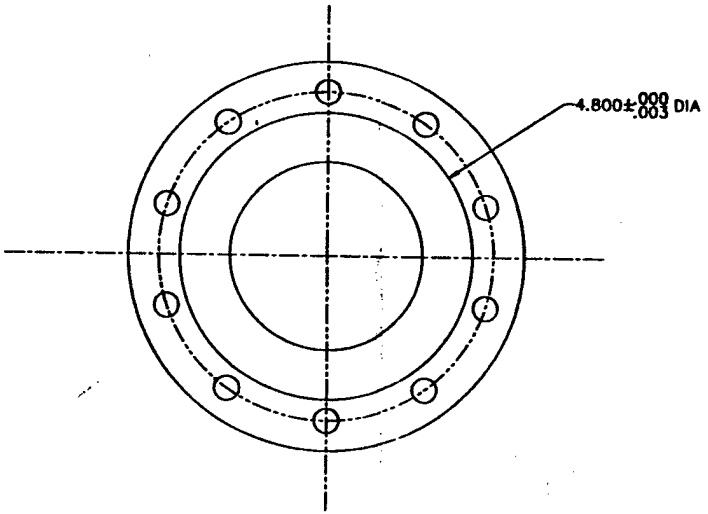

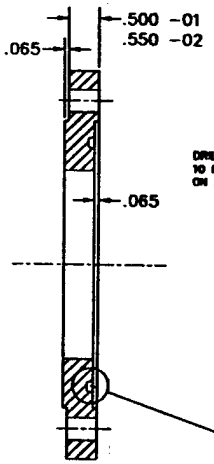

OUTER CONDUCTOR SPACER
(part #10)

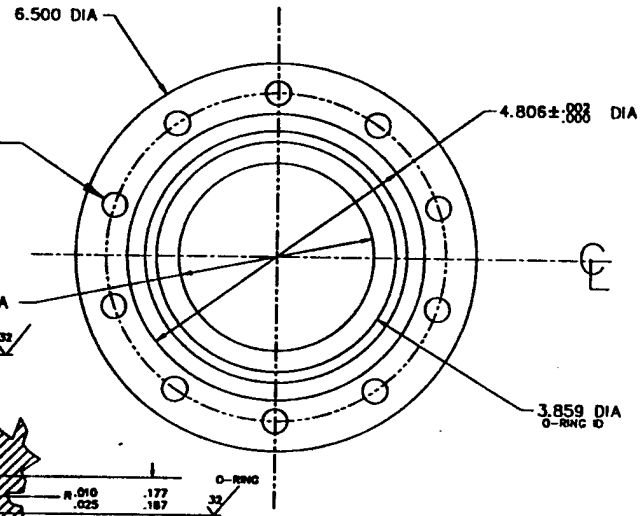

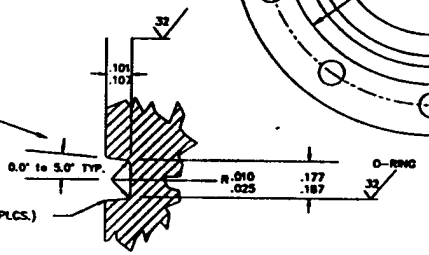

O-RING DETAIL #2

NOT TO SCALE
PARKER O-RING #2-241

ITEM	QTY	PART NUMBER	DESCRIPTION	MATERIAL
1	1	6061-T6		ALUM ALLOY

PARTS LIST

DO NOT SCALE DRAWING

CONTRACT NO. 8090

APPROVALS	DATE
D.E.ELLIBEE	10/9/97

EG&G MSI
ALBUQUERQUE OPERATIONS

TITLE: OUTER COAXIAL ADAPTER

SIZE D | CAGE CODE 29674 | DWG NO. 124713 | REV

SCALE | SHEET

124713

NOTE:
1 – Break all edges

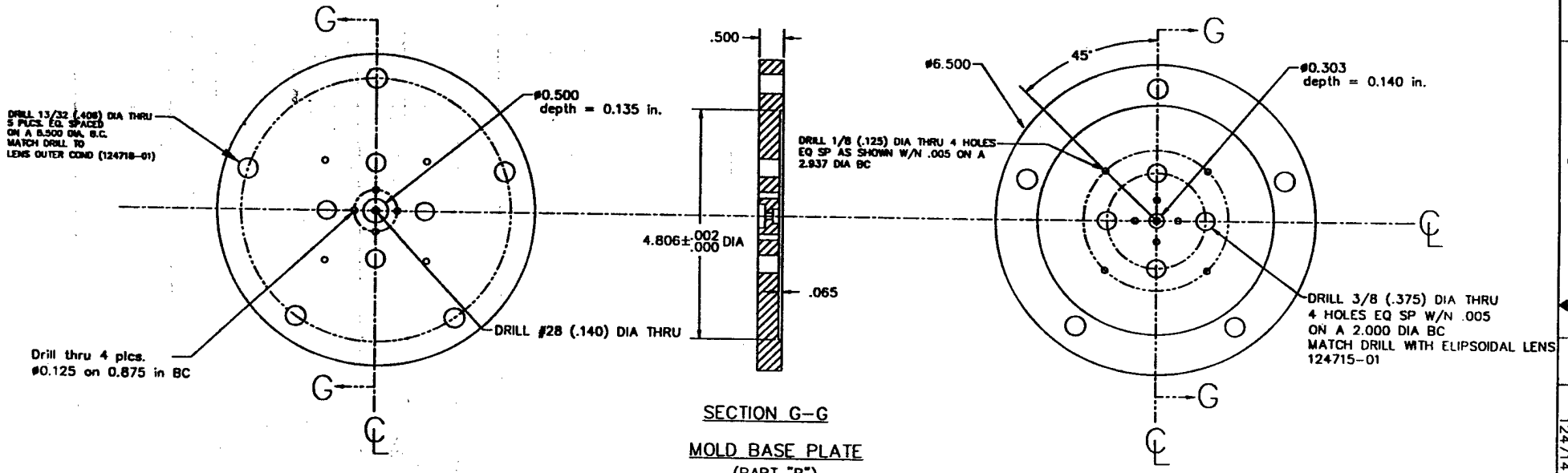

SECTION G–G

MOLD BASE PLATE
(PART "B")

1		6061–T6	ALUM ALLOY	1

PARTS LIST

DO NOT SCALE DRAWING

CONTRACT NO.	8090
APPROVALS	DATE
D.E.ELLIBEE	10/8/92

EG&G MSI
ALBUQUERQUE OPERATIONS

MOLD BASE PLATE

SIZE D	FSCM NO. 29674	DWG NO. 124714

SCALE

SHEET OF

124714

NOTE:
1 – Break all edges
2 – MATERIAL = TEFLON

ELIPSOIDAL SURFACE IN INCHES								
X	Y		X	Y		X	Y	
0	1.575		0.932	1.373		1.864	0.313	
0.019	1.575		0.951	1.364		1.883	0.222	
0.038	1.575		0.97	1.355		1.902	0	
0.057	1.574		0.989	1.345				
0.076	1.574		1.008	1.335				
0.095	1.573		1.027	1.326				
0.114	1.572		1.046	1.315				
0.133	1.571		1.065	1.306				
0.152	1.57		1.084	1.294				
0.171	1.568		1.103	1.283				
0.19	1.567		1.122	1.272				
0.209	1.565		1.141	1.26				
0.228	1.563		1.16	1.248				
0.247	1.562		1.179	1.236				
0.266	1.559		1.198	1.223				
0.285	1.557		1.217	1.21				
0.304	1.555		1.236	1.197				
0.323	1.552		1.255	1.183				
0.342	1.549		1.274	1.169				
0.361	1.546		1.293	1.155				
0.38	1.543		1.312	1.14				
0.399	1.54		1.331	1.125				
0.418	1.536		1.35	1.109				
0.437	1.533		1.369	1.093				
0.456	1.529		1.388	1.076				
0.475	1.525		1.407	1.059				
0.494	1.521		1.426	1.042				
0.513	1.516		1.445	1.024				
0.533	1.512		1.464	1.005				
0.552	1.507		1.483	0.986				
0.571	1.502		1.502	0.966				
0.59	1.497		1.521	0.945				
0.609	1.492		1.54	0.924				
0.628	1.487		1.56	0.901				
0.647	1.481		1.579	0.878				
0.666	1.475		1.598	0.855				
0.685	1.469		1.617	0.83				
0.704	1.463		1.636	0.804				
0.723	1.457		1.655	0.778				
0.742	1.45		1.674	0.749				
0.761	1.443		1.693	0.718				
0.78	1.436		1.712	0.686				
0.799	1.429		1.731	0.653				
0.818	1.422		1.75	0.617				
0.837	1.414		1.769	0.579				
0.856	1.406		1.788	0.537				
0.875	1.398		1.807	0.492				
0.894	1.39		1.826	0.441				
0.913	1.382		1.845	0.383				

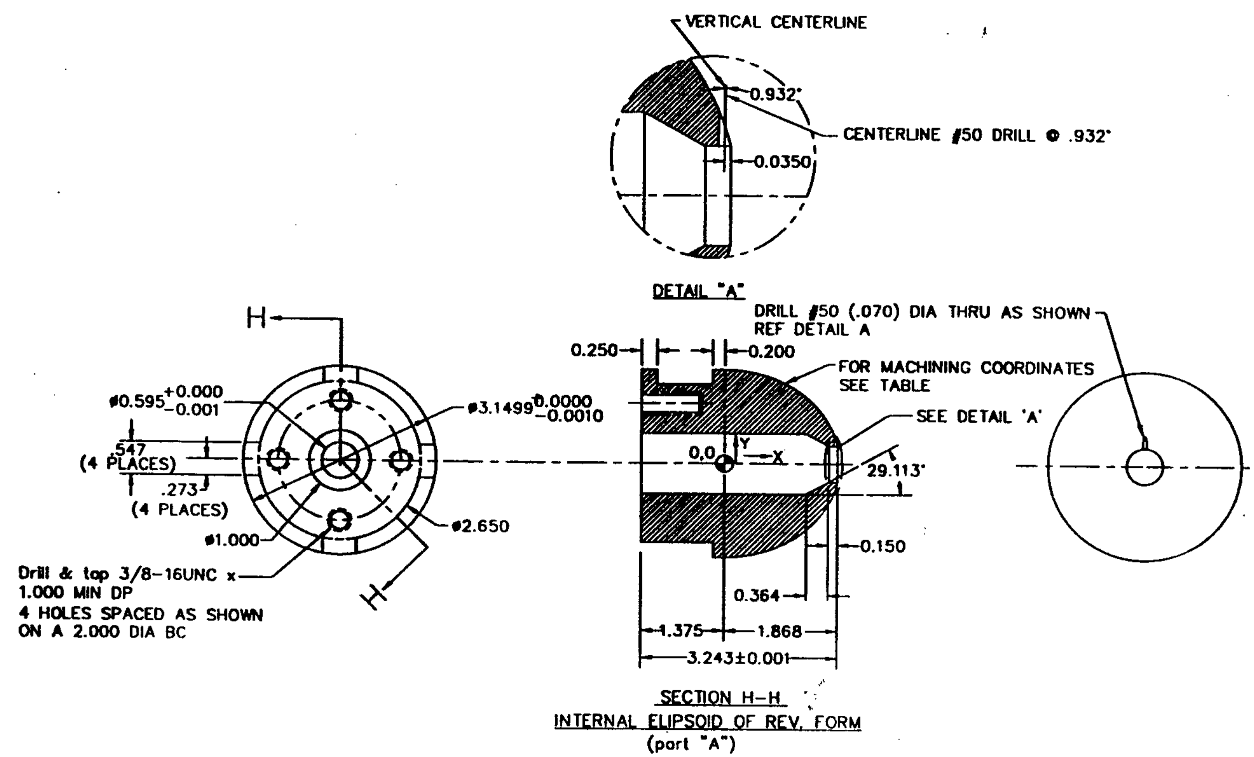

CONTRACT NO. 8090	EG&G MSI ALBUQUERQUE OPERATIONS	
DRAWN D.E.ELLIBEE 10/8/97	LENS ELIPSOIDAL MOLD FORM	
SIZE D	CAGE CODE 29674	DWG NO. 124715

DO NOT SCALE DRAWING

124715

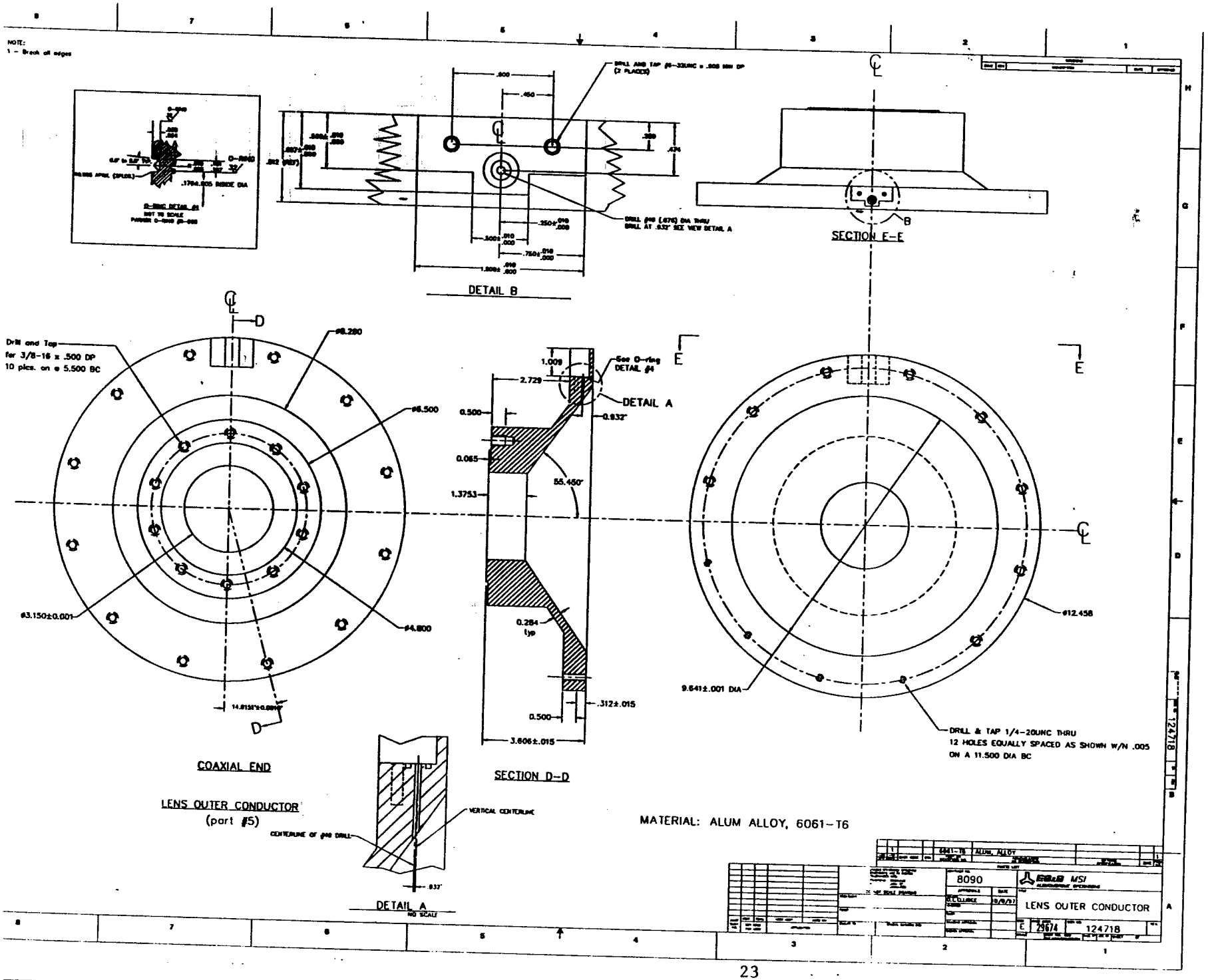
NOTE:
1 – Break all edges
DETAIL B
SECTION E–E
Drill and Tap
for 3/8–16 x .500 DP
10 plcs. on ø 5.500 BC
ø8.280
ø6.500
ø4.800
ø3.150±0.001
COAXIAL END
LENS OUTER CONDUCTOR
(part #5)
See O-ring
DETAIL #4
DETAIL A
2.729
1.009
0.932"
0.500
0.065
1.3753
55.450°
0.284
typ
.312±.015
0.500
3.606±.015
SECTION D–D
ø12.458
9.641±.001 DIA
DRILL & TAP 1/4–20UNC THRU
12 HOLES EQUALLY SPACED AS SHOWN W/N .005
ON A 11.500 DIA BC
VERTICAL CENTERLINE
CENTERLINE OF ø40 DRILL
.937
DETAIL A
NO SCALE
MATERIAL: ALUM ALLOY, 6061–T6
6061-T6
ALUM. ALLOY
8090
MSI
LENS OUTER CONDUCTOR
E
29674
124718

NOTE: Break all edges

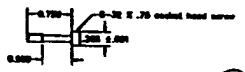

(part #4) ②

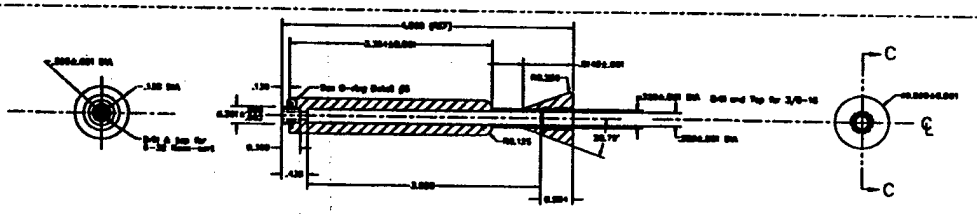

SECTION C–C

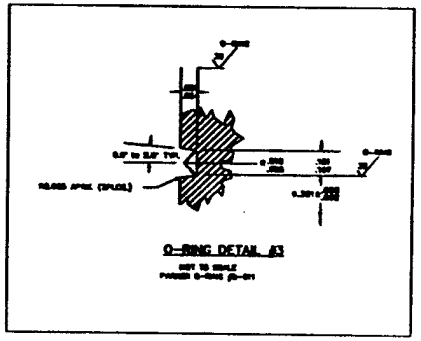

O-RING DETAIL #3

Lens Center Conductor ①

(part #3)

1				SCR, SOC HD, #8-32UNC x 3/4" L	2
1			6061-T6	ALUM ALLOY	1

PARTS LIST

DO NOT SCALE DRAWING

CONTRACT NO.	8090
APPROVALS	DATE
D.F. ELWREE	10/7/92

EG&G MSI
ALBUQUERQUE OPERATIONS

TITLE: HIRA CENTER CONDUCTORS

SIZE	CAGE CODE	DWG NO.	REV.
D	29674	124712	

SCALE | DRAWN | APP'D | SHEET 1 OF

NOTE:

1- BREAK ALL EDGES

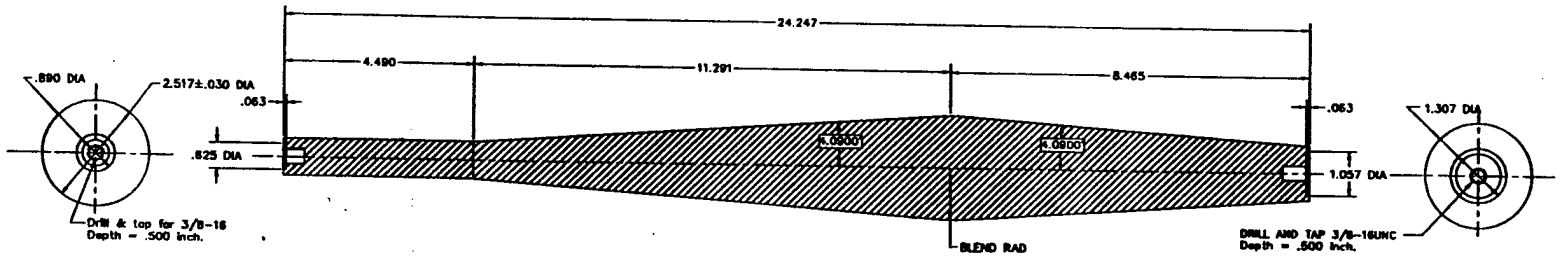

FEED ARM ②

(PART #11) (MAKE 2 EA)

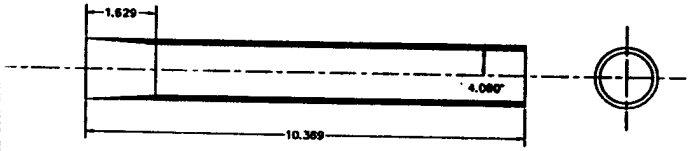

ARM INSULATOR ①

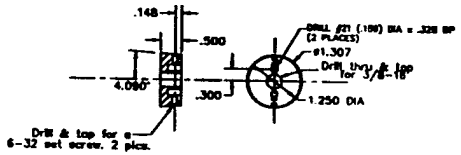

RESISTOR INSIDE CAP ③

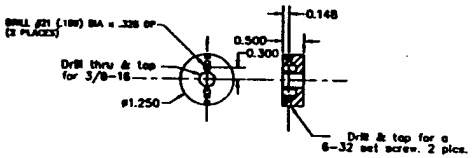

RESISTOR END CAP ④

3	6061-T6	ALUM ALLOY	
2	6061-T6	ALUM ALLOY	
1	6061-T6	ALUM ALLOY	
C-10		FIBERGLASS	

DRAWN	
CHECKED	
APPROVED	
DATE	

EB&G MSI

FEED ARM

E 29674 124720

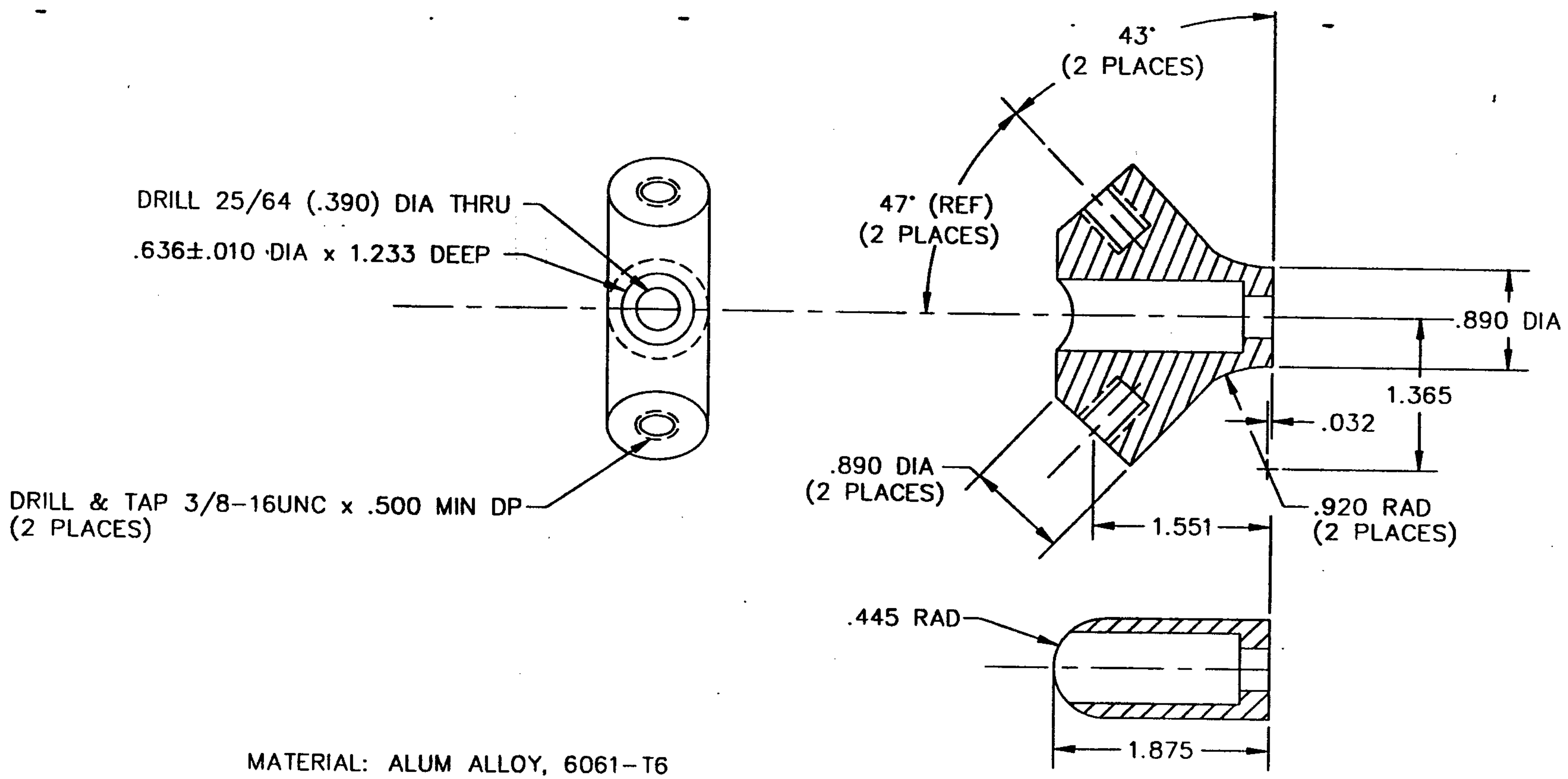

MATERIAL: ALUM ALLOY, 6061-T6

EG&G MSI
ALBUQUERQUE OPERATIONS

TITLE: CAP

SIZE	CAGE CODE	DWG NO.	REV.
B	29674	124721	

DRAWN: GROSBIER — DATE: XX-XX-XX

UNLESS OTHERWISE SPECIFIED DIMENSIONS ARE IN INCHES

DO NOT SCALE DRAWING

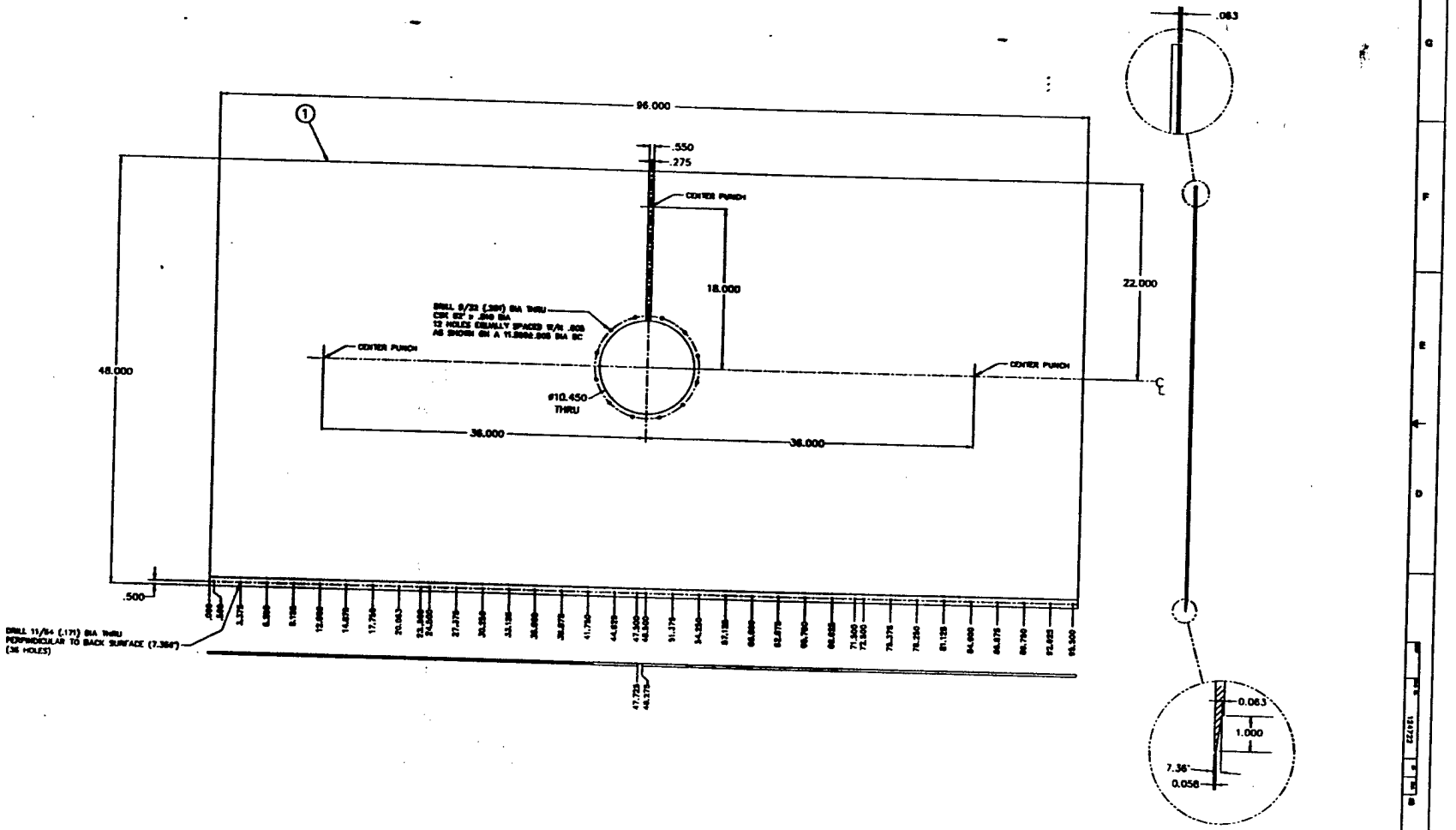
96.000
.550
.275
CENTER PUNCH
18.000
22.000
48.000
CENTER PUNCH
CENTER PUNCH
Ø10.450
THRU
36.000
36.000
.500
.063
0.063
1.000
7.36°
0.056
GROUND PLANE

REVISIONS				
ZONE	REV	DESCRIPTION	DATE	APPROVED

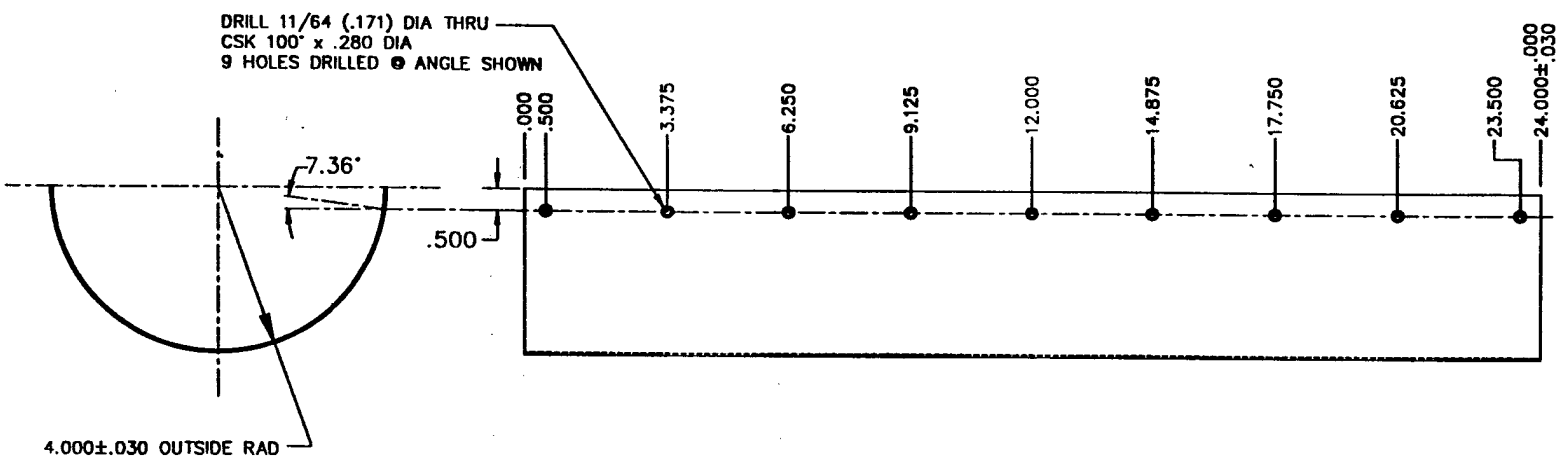

QTY REQD -20	QTY REQD -16	CAGE CODE	SYM	PART OR IDENTIFYING NO.	NOMENCLATURE OR DESCRIPTION	MATERIAL SPECIFICATION	ZONE	ITEM NO.
	1			5052-H32	ALUM ALLY, .063 THK			1

PARTS LIST

UNLESS OTHERWISE SPECIFIED DIMENSIONS ARE IN INCHES TOLERANCES ARE: FRACTIONAL ± DECIMALS .XX ± .010 .XXX ± .005

DO NOT SCALE DRAWING

CONTRACT NO.

APPROVALS	DATE
GROSBIER	91-10-24

EG&G MSI
ALBUQUERQUE OPERATIONS

TITLE
GROUND PLANE REFLECTOR

SIZE	CAGE CODE	DWG. NO.	REV.
C	29674	124738	

SCALE 1/2 | SHEET

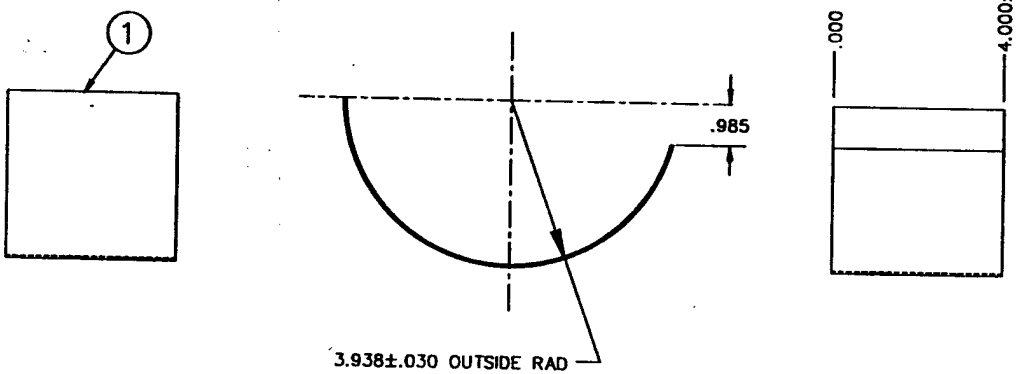

REVISIONS				
ZONE	REV	DESCRIPTION	DATE	APPROVED

QTY REQ'D -20	QTY REQ'D -10	CAGE CODE	STK	PART OR IDENTIFYING NO.	NOMENCLATURE OR DESCRIPTION	MATERIAL SPECIFICATION	ZONE	ITEM NO.
1	1			5052-H32	ALUM, ALLOY, .063 THK			2
1	1							1

PARTS LIST

DO NOT SCALE DRAWING

CONTRACT NO.

APPROVALS	DATE
GROSBIER	91-10-24

EG&G MSI
ALBUQUERQUE OPERATIONS

TITLE: REFLECTOR BACK PLATE

SIZE C | CAGE CODE 29674 | DWG. NO. 124739 | REV.

SCALE 1/2 | SHEET 1 OF

DWG. NO. 124739 | REV. A

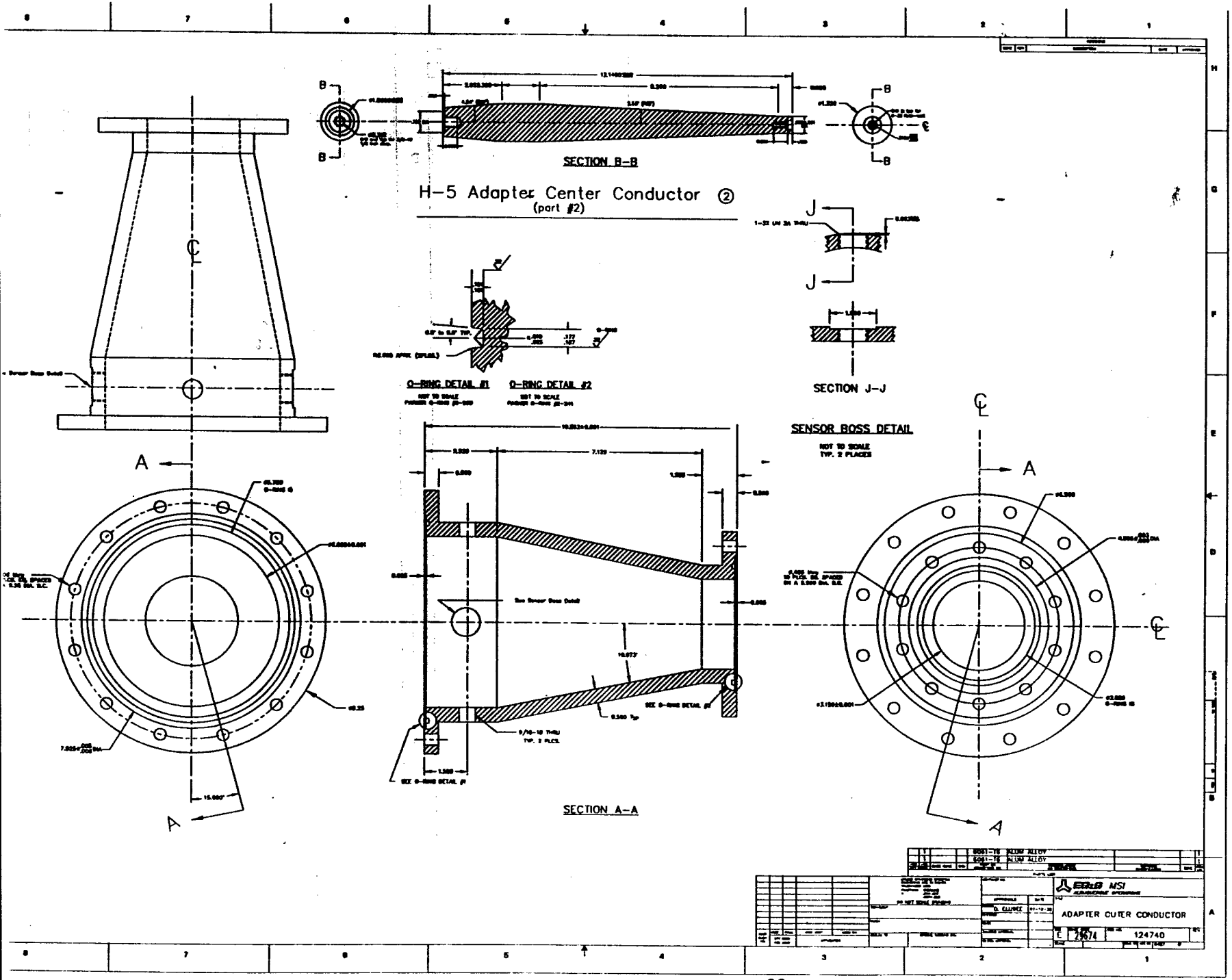
SECTION B-B
H-5 Adapter Center Conductor ②
(part #2)
O-RING DETAIL #1
O-RING DETAIL #2
SECTION J-J
SENSOR BOSS DETAIL
NOT TO SCALE
TYP. 2 PLACES
SECTION A-A
6061-T6 ALUM ALLOY
ADAPTER OUTER CONDUCTOR
124740

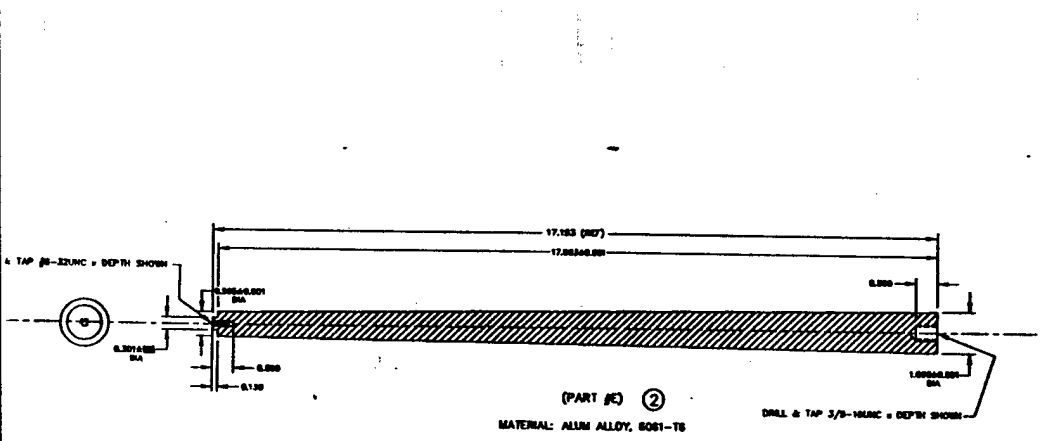

(PART #C) ②

MATERIAL: ALUM ALLOY, 6061-T6

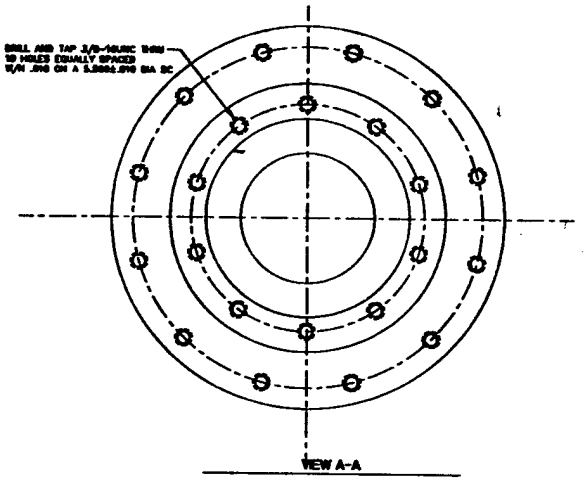

VIEW A-A

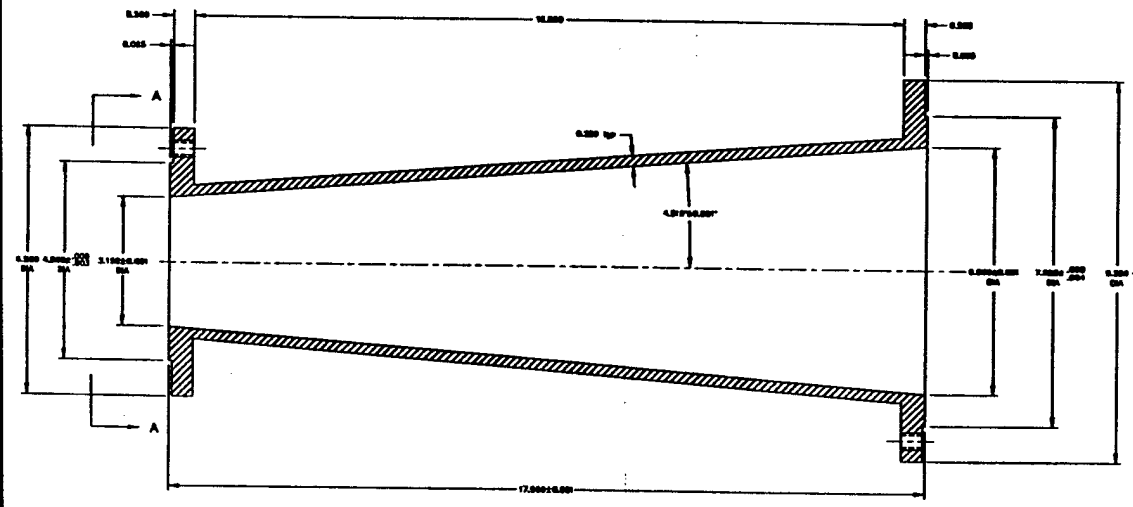

(PART #C) ①

MATERIAL: ALUM ALLOY, 6061-T6

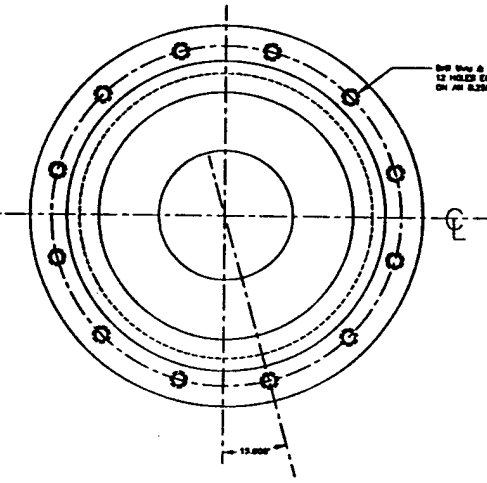

2	6061-T6	ALUM ALLOY	
1	6061-T6	ALUM ALLOY	

SBRC MSI

LENS TEST ADAPTER (PART 2)

E 29674 124741

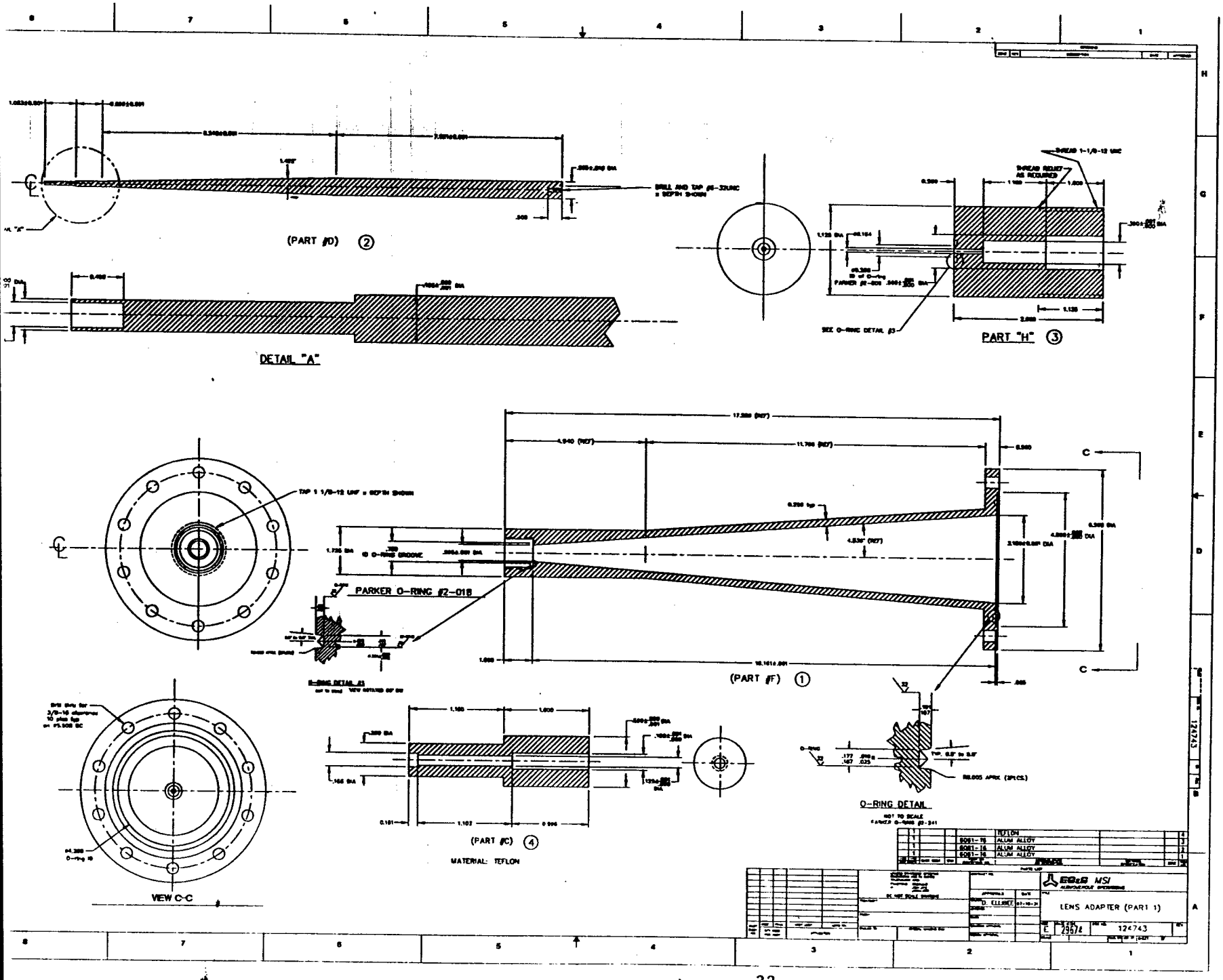
(PART #D) ②
DETAIL "A"
PART "H" ③
PARKER O-RING #2-018
(PART #F) ①
(PART #C) ④
MATERIAL: TEFLON
VIEW C-C
O-RING DETAIL
TEFLON
6061-T6 ALUM ALLOY
6061-T6 ALUM ALLOY
6061-T6 ALUM ALLOY
EG&G NSI
LENS ADAPTER (PART 1)
124743

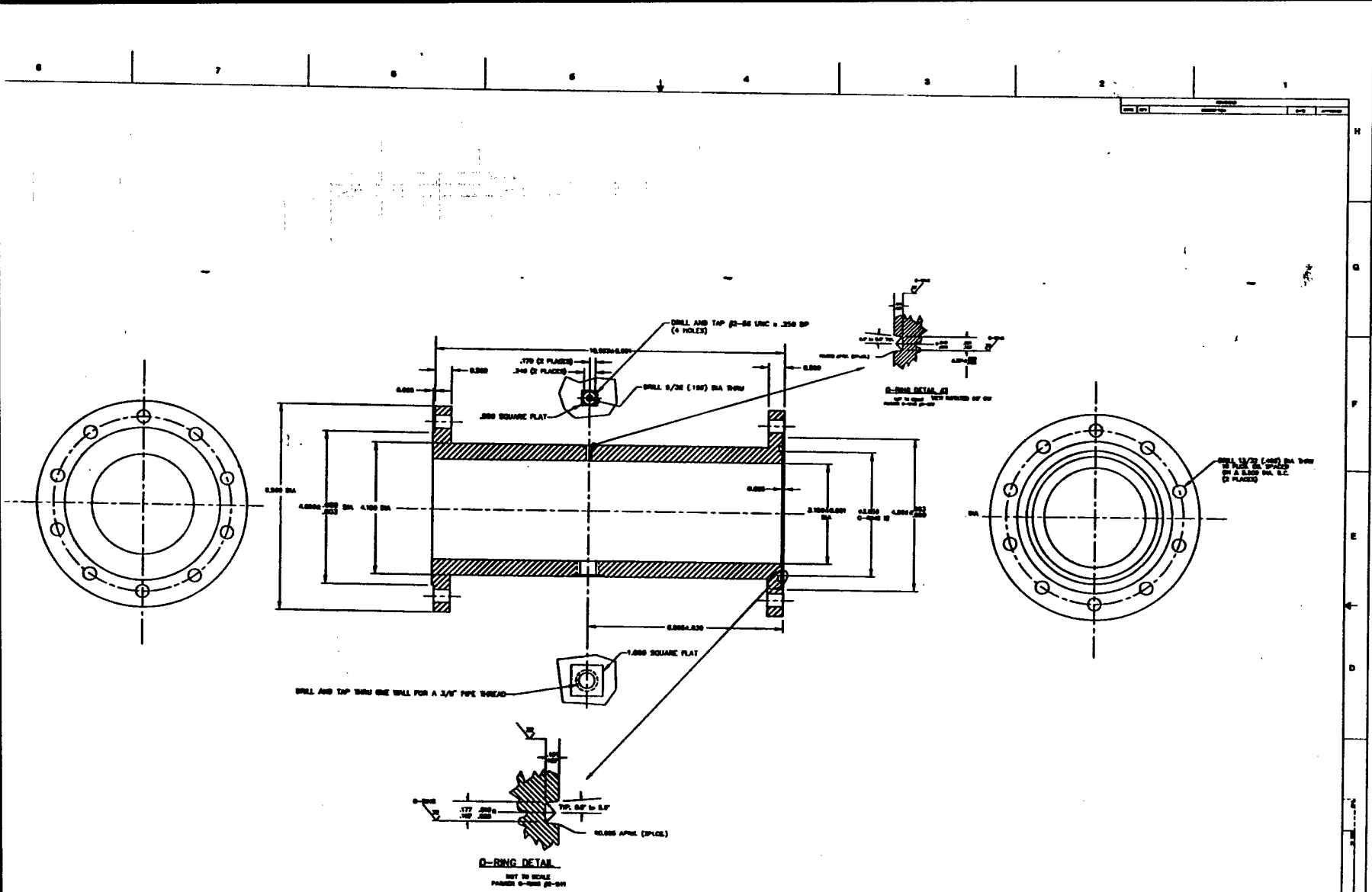
O-RING DETAIL
6061-T6 ALUM ALLOY
ADAPTER
124752

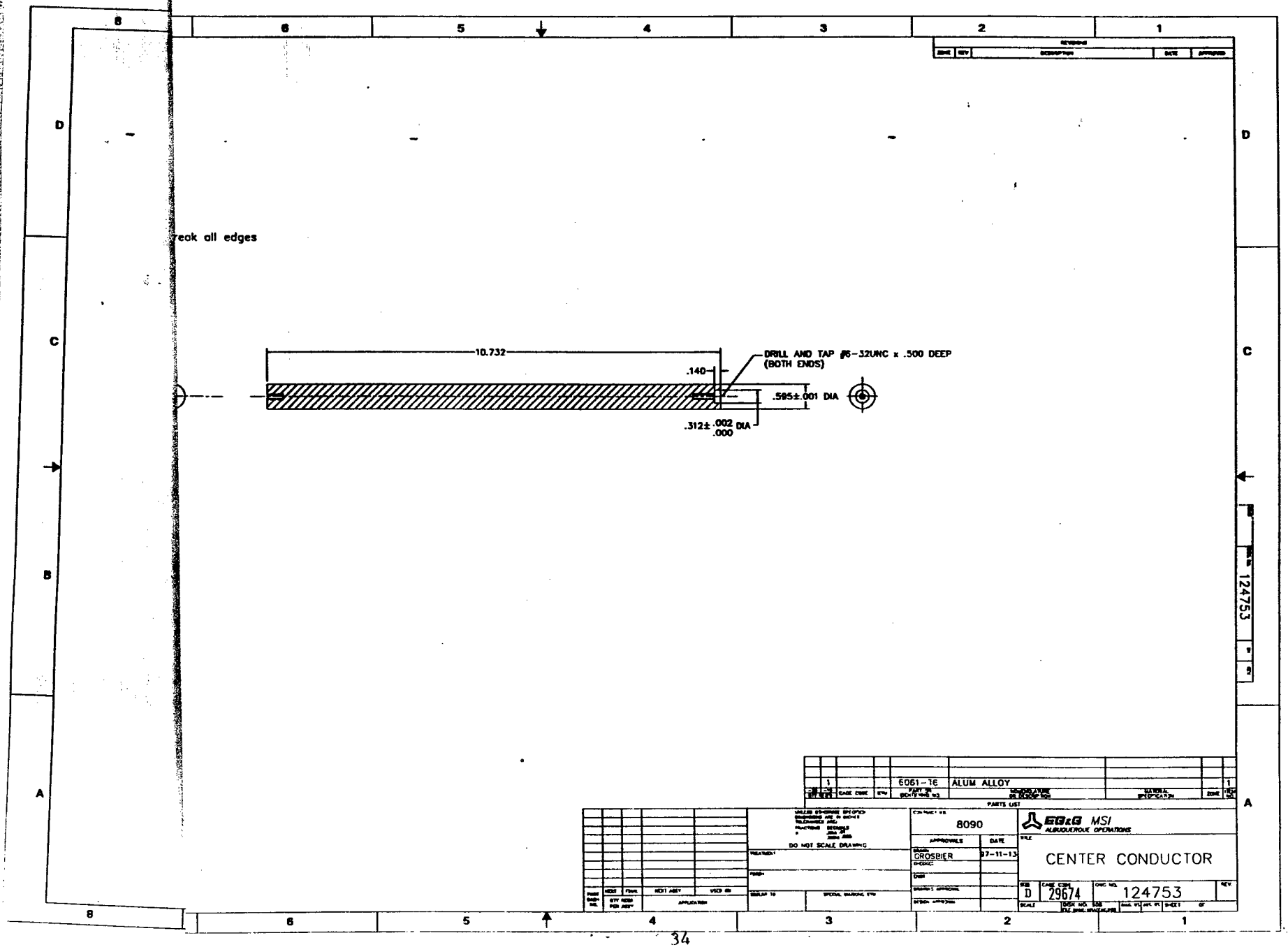
reak all edges
10.732
.140
DRILL AND TAP #6-32UNC x .500 DEEP
(BOTH ENDS)
.595±.001 DIA
.312± .002 .000 DIA
6061-T6
ALUM ALLOY
8090
DO NOT SCALE DRAWING
CROSBIER
97-11-13
GE&G MSI
ALBUQUERQUE OPERATIONS
CENTER CONDUCTOR
D
29674
124753

REVISIONS				
ZONE	REV	DESCRIPTION	DATE	APPROVED

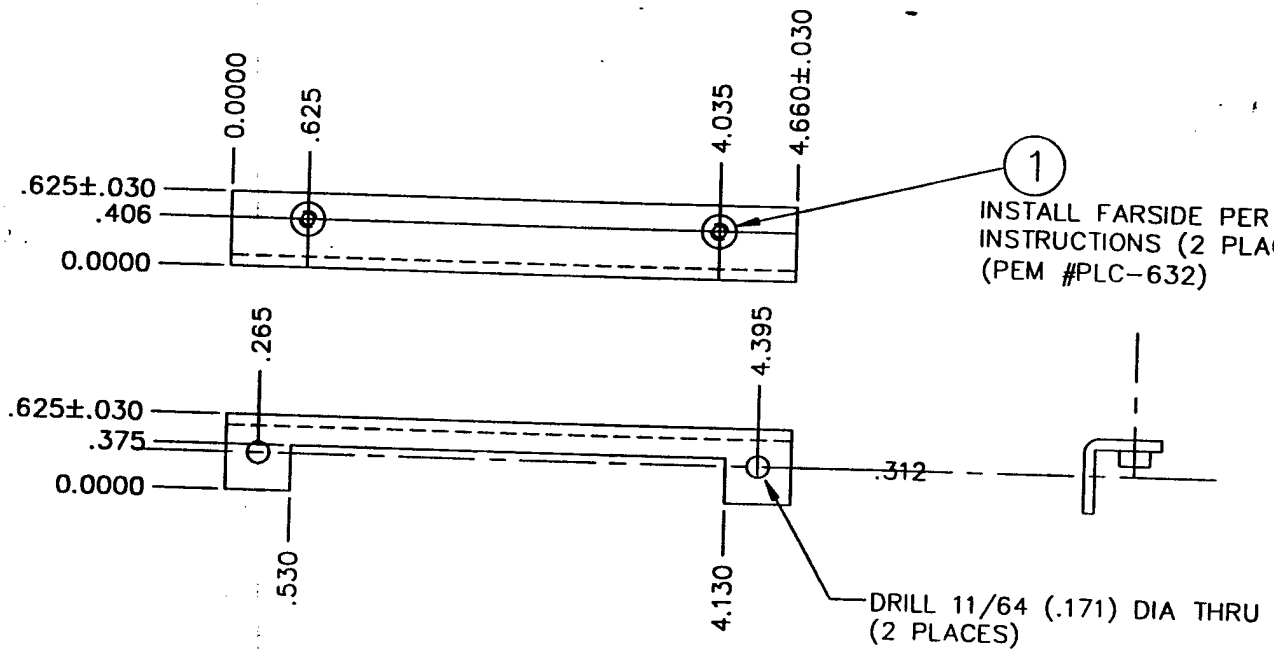

MATERIAL: ALUM, .093 THK, 5052-H32

PART DASH NO.	NEXT	FINAL	NEXT ASSY	USED ON
	QTY REQD PER ASSY		APPLICATION	

UNLESS OTHERWISE SPECIFIED DIMENSIONS ARE IN INCHES
TOLERANCES ARE:
FRACTIONS ± DECIMALS .XX± .XXX±
DO NOT SCALE DRAWING
TREATMENT
FINISH ALODINE
SIMILAR TO | SPECIAL MARKING SYM.

CONTRACT NO.

APPROVALS	DATE
DRAWN GROSBIER	XX-XX-XX
CHECKED	
ENGR	
DRAWING APPROVAL	
DESIGN APPROVAL	

EG&G MSI
ALBUQUERQUE OPERATIONS

TITLE
FAN BRACKET

SIZE	CAGE CODE	DWG NO.	REV.
B	29674	124754	

SCALE | DISK NO: | CALC. WT | ACT. WT | SHEET | OF

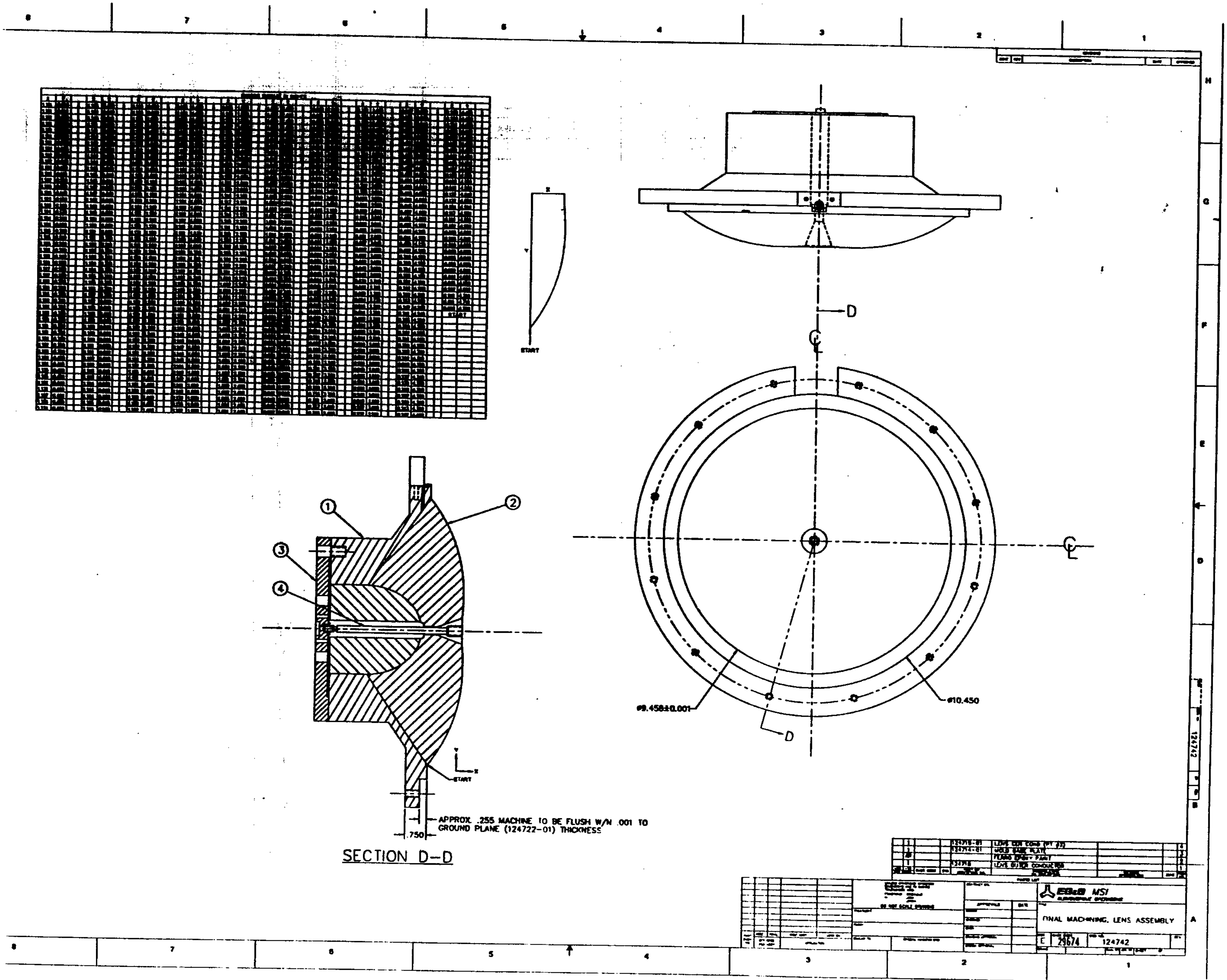
SECTION D–D
APPROX. .255 MACHINE TO BE FLUSH W/N .001 TO GROUND PLANE (124722-01) THICKNESS
.750
START
ø9.458±0.001
ø10.450
D
EG&G MSI
FINAL MACHINING, LENS ASSEMBLY
29674
124742

DISTRIBUTION LIST

AUL/LSE Bldg 1405 - 600 Chennault Circle Maxwell AFB, AL 36112-6424	1 cy
DTIC/OCP 8725 John J. Kingman Rd, Suite 0944 Ft Belvoir, VA 22060-6218	2 cys
AFSAA/SAI 1580 Air Force Pentagon Washington, DC 20330-1580	1 cy
AFRL/PSTL Kirtland AFB, NM 87117-5776	2 cys
AFRL/PSTP Kirtland AFB, NM 87117-5776	1 cy
Farr Research, Inc. 614 Paseo Del Mar NE Albuquerque, NM 87123	1 cy
Official Record Copy AFRL/DEHP/William Prather	5 cys